Annu. Rev. Earth Planet. Sci. 2000. 28:419–75

NEW PERSPECTIVES ON ORBITALLY FORCED STRATIGRAPHY

Linda A. Hinnov
Department of Earth and Planetary Sciences, Johns Hopkins University, Baltimore, Maryland 21218

Key Words Milankovitch theory, cyclic stratigraphy, Earth's orbital parameters

■ **Abstract** This survey of the current status of research into Earth's orbitally forced paleoclimatic record summarizes recent developments in the theory of Earth's orbital parameters, and reviews how various techniques of data collection and analysis have fared in the search and recovery of orbital signals in ancient stratigraphy. The emerging significance of the quasi-periodicity of Earth's orbital variations as a principal tool in the analysis of orbitally forced stratigraphy is discussed in detail. Five case studies are presented that illustrate new directions in research: (*a*) time series analysis of discontinuous strata; (*b*) measurement of ultra-high resolution stratigraphic signals; (*c*) new perspectives on the 100 kyr Pleistocene glaciation problem; (*d*) stratigraphic evidence for solar system resonance modes; and (*e*) evaluating Phanerozoic length of day from orbitally forced stratigraphy.

1. INTRODUCTION

1.1 New Perspectives

The study of how Earth's orbital parameters came to be recorded in ancient stratigraphy has recently moved into a new phase of scientific inquiry and discovery. Notable advances in celestial mechanics and in the analysis of stratigraphic data have given rise to new ways of solving old problems, and have uncovered new problems for the first time. New tools have facilitated the recovery of extended, high-resolution orbital signals from stratigraphy. Advanced analytical techniques have now been fully incorporated into the field. An updated theory of Earth's orbital parameters provides an accurate ephemeris for the past 16 million years, for precision correlation between Earth's orbital parameters and orbitally forced stratigraphy. Some orbital eccentricity modes can be used for orbital-stratal calibrations to several hundred million years ago.

These breakthroughs have transformed the study of orbitally forced stratigraphy into an applied field that addresses long-standing problems in disciplines as far-ranging as geochronology, geodynamics, and astrodynamics. Orbital signals provide the framework for a high-resolution orbital chronostratigraphy as far back

as the Miocene (Berggren et al 1995, Hilgen et al 1999). The recognition of orbital frequencies in Mesozoic sections has led to the construction of high-resolution ''floating'' time scales for entire geologic epochs (e.g. Herbert et al 1995, Shackleton et al 1999a). The state of Earth's dynamical ellipticity can be evaluated through geophysical modeling of high-fidelity stratigraphy (e.g. Thomson 1991, Lourens et al 1996). Exploration of solar system resonance is now possible with the collection of multimillion year–long stratigraphic sequences extending into more remote geological times (Beaufort 1994, Lourens & Hilgen 1997, Shackleton et al 1999b, Olsen & Kent 1999). These achievements, together with many others, form the vanguard of a new generation of studies that has outpaced the expectations of the scientific community.

This paper reviews the current status of the theory of orbital variations and its application to estimating Earth's orbitally forced solar radiation (Section 2), and describes and applies new techniques for probing the geologic record for evidence of orbital signals (Section 3). Emphasis is placed on the nature of the orbital input, observations of stratigraphic output, and analytical tools that have been developed to link them. The five case studies in Section 3 illustrate some of the pure and applied problems that have been addressed recently, and showcase exemplary cyclic stratigraphy from the Cenozoic, Mesozoic, and Paleozoic eras. Section 3.1 discusses typical problems faced by researchers investigating ancient cyclic strata, and applies strategies that have been recently developed to handle these problems to the Jurassic Domaro Limestone. Section 3.2 explores the limits of stratigraphic sampling and orbital to sub-orbital signal imaging of bathyal carbonates from the Cretaceous Piobbico core. Section 3.3 describes the recent methodology shift from the analysis of orbital signals to the analysis of long-period modulations in orbital signals, and how this has shed new light on the origin of the Late Pleistocene 100 kyr glaciations. In Section 3.4, the theme of long-period modulations in Earth's obliquity and precession index is explored in the context of resonance modes between the orbits of Earth and Mars. Finally, Section 3.5 examines the still somewhat schematic subject of tidal dissipation in the Earth-Moon system and the geological evolution of Earth's precession rate *k*.

1.2 Recent Accomplishments

1.2.1 Developments in Orbital Theory During the late 1980s and throughout the 1990s, innovations in celestial mechanics revolutionized our understanding of the Solar System (for a historical account, see Peterson 1993). New computational approaches to the general problem of secular planetary motion have led to new insights into the long-term evolution of the Solar System, and to the discovery of major interactions (''resonances'') among the planets and of a history of chaotic motions (e.g. Laskar 1988, 1989, 1990, 1992; Quinn et al 1991; Sussmann & Wisdom 1992; Murray & Holman 1999). Astrogeodynamical factors, including a visco-elastic Earth, Earth-Moon interactions, and relativistic effects, are now all included in the new theory (Laskar et al 1993). Sensitivity experiments

have supplied quantitative information on model time validity; this is important for understanding the theoretical limits for precision-calibration of orbitally forced stratigraphy through geologic time (Laskar 1999). Stratigraphers need to be aware of these new developments as they formulate hypothesis tests for their data; aspects of the updated theory that are most likely to pertain to orbitally forced stratigraphy are reviewed in Section 2.1.

1.2.2 Earth's Orbitally Forced Insolation At every point on Earth, the incoming solar radiation (insolation) varies at diurnal and annual time scales, and is weighted and modulated by Earth's orbital parameters (e.g. Berger et al 1993). Rubincam (1994) recast the classical insolation equation as a spherical harmonic expansion to facilitate the computation of insolation over any time scale at any geographical location. Orbital-scale variations in insolation take on different amplitudes and frequencies depending on geographical latitude, season, and time of day (Berger et al 1993). Some of these variations are relatively unexplored, yet are extremely important; these are reviewed in Section 2.2. With its passage through the atmosphere, insolation experiences heavy ''filtering'' upon encountering land-sea-ice variations in albedo and emissivity, along with global heat transport (e.g. North et al 1981). This, and the cascade of environmental responses that transforms this filtered insolation into stratigraphic signal, has been the subject of dozens of studies (see summaries in Crowley & North 1991, Allen et al 1993, Bradley 1999, and references therein).

1.2.3 Orbitally Forced Stratigraphy Since the seminal study of the Late Pleistocene by Hays et al (1976), stratigraphers have been searching for evidence of orbitally forced climate throughout Earth's history. The sedimentological and stratigraphic literature of the 1980s and 1990s is filled with countless publications that conclude that orbital forcing was probably a principal mechanism in the accumulation of many thin-bedded (dm-m scale) cyclic stratigraphic formations of all geologic ages. These formations represent a wide variety of climatically sensitive (usually biogenic carbonate-rich) facies, indicating a broad range of responsive behaviors of sedimentary environments to orbitally forced climate. Although the majority of data are from marine-based strata, high-quality continental records have now also been recovered: e.g. the 500 kyr-long Devil's Hole vein calcite series (Winograd et al 1992), the *ca.* 1.0 Myr-long Pleistocene palynological series from former Lake Bogotà, Colombia (e.g. Hooghiemstra et al 1993) and Macedonia, Greece (Mommersteeg et al 1995), the 2.4 Myr-long Chinese loess records (e.g. Kukla et al 1990, Kukla & Cilek 1996), the 5 Myr-long Lake Baikal biogenic silica record (Williams et al 1997), the spectacular *ca.* 40 Myr-long Late Triassic–Early Jurassic Newark Basin series of eastern North America (Olsen 1997), and the Late Pleistocene ice cores from both poles (e.g. Jouzel et al 1987, Grootes et al 1993, Petit et al 1999) as well as from middle latitude continental interiors (e.g. Thompson et al 1997). Now, near-continuous coverage of orbitally forced stratigraphy is provided as far back as the Oligocene

Epoch. For earlier, pre-Cenozoic times, the recovered record is still fragmentary, although some measured sections span entire geologic stages representing many millions of years of apparently continuous, orbitally forced stratigraphy. Because the accuracy of the orbital theory does not permit direct calibration between pre-Cenozoic stratigraphy and orbital signals, interpretation of these older sequences is restricted to general statistical comparisons between data and orbital theory. There is hope, however, that stratal-orbital calibrations can be accomplished using certain eccentricity modes (Shackleton et al 1999a).

1.2.4 New Tools A number of geophysical logging tools have been enlisted in the effort to recover affordable, long, continuous, and high-resolution stratigraphic signals—among these are sonic velocity, resistivity, natural gamma ray, neutron density, infrared and near-ultraviolet spectroscopy, wet bulk-density, gamma ray attenuation porosity evaluation (GRAPE), magnetic susceptibility, and optical densitometry (e.g. Jarrard & Arthur 1989; Herbert & Mayer 1991; DeMenocal et al 1991; Herbert et al 1992; Melnyk et al 1994; Yang et al 1995; Weedon et al 1997; Grippo et al 1998, 1999). The outputs from these tools are statistically correlated to physical and chemical properties in sediment. This stands in contrast to the detailed experimental knowledge of the physico-chemical behavior of oxygen isotopes culled from foraminifera in connection with the Pleistocene deep sea coring project. On the other hand, the cost of producing detailed stable isotope series is high, and is of limited value in older stratigraphies where diagenesis has wiped out primary isotopic signals. In this respect, one logging tool that has proved successful in recovering extraordinarily high-resolution stratigraphic information is optical densitometry (Herbert & Fischer 1986; Bond et al 1992; D'Argenio et al 1998; Grippo et al 1998, 1999; Section 3.2). Another simple and highly effective strategy for quantifying cyclic stratigraphy relies on the recognition and documentation of two or more depositional facies that occur in a repetitive stratigraphic pattern. Each facies is ''ranked'' by a number and recorded as a function of stratigraphic position. This technique was introduced by Olsen (1984) as a means to quantify the famous Van Houten cycles in the Triassic Newark Basin series. Similarly, Weedon (1989) recorded Jurassic pelagic limestone/shale cycles with ranks of 0 and 1. These digitized representations can be submitted to time series analysis, although rank series discontinuities are not always compatible with Fourier-based analysis (Weedon 1989), and facies-dependent accumulation rates can obscure underlying orbital signals (Hinnov & Park 1998; see also Section 3.1.3).

1.3 Outstanding Problems

1.3.1 Time Scale Recovery The most difficult problem in the analysis of orbitally forced stratigraphy is depth-to-time transformation. Accurate and precise geochronology is essential for a meaningful determination of stratigraphic time-periodicity. Ideally, high-precision geochronometers should be collected

from specific levels within the stratigraphy. Magnetostratigraphy has been essential for correlations to the high-precision polarity chrons of the Cenozoic geomagnetic polarity time scale. For stratigraphy older than Late Cretaceous, reliance on standard biozonations is crucial for correlations usually to a sparsely sampled and imprecise geochronometric database. Also, an emerging Mesozoic global chemostratigraphy may soon prove to be useful as a high-resolution correlation device in cases of ambiguous or missing fossil evidence (e.g. Jenkyns 1988, Bartolini et al 1996, Zempolich & Erba 2000).

For Mesozoic and older sections, a number of radioisotope geochronometers can define stratigraphic intervals that are only a few million years in duration. For example, the $^{40}Ar/^{39}Ar$ laser fusion approach determined sanidine ages to within ± 0.5 Myr in the bentonites of the Cretaceous Western Interior Seaway (Obradovich 1993). The single zircon crystal U/Pb isotope dilution dating method yields similarly high precision dates (e.g. Bowring et al 1993); however, special care must be taken in screening the crystals for hidden inheritance or other compositional zoning features (Hanchar & Miller 1993, Hanchar & Rudnick 1995, Miller et al 1998), or for evidence of Pb loss (e.g. Mezger & Krogstad 1997). These problems could explain, for example, the conflict between single zircon dates indicating that the Triassic Latemar cyclic carbonate platform was deposited in 2–4 Myrs (Brack et al 1996, 1997; Mundil et al 1996), as opposed to cyclostratigraphic and sedimentologic analysis indicating an orbitally forced deposition of the limestone over a *ca.* 10–12 Myr period (Goldhammer et al 1987, Hinnov et al 1997, Hardie & Hinnov 1997, Kerr 1999).

1.3.2 Sampling and Stratigraphic Completeness A chronic problem in stratigraphic signal recovery involves the choice of sampling interval. The statistical (Nyquist) rule that a cycle needs to be sampled at least twice can be inadequate when one is first assessing stratigraphy. Estimating an average or median thickness of the principal cycle of interest and applying the Nyquist rule to set up a sampling grid guarantees that at least half of the cycles will be undersampled. The obvious remedy is always to sample at an extremely high rate. In this regard, tools with high-resolution capability, such as optical densitometry (see Section 3.2), may prove to be most useful and affordable for the highest-resolution collection of long stratigraphic series. Also, a uniform sampling grid may not always be the best data-gathering procedure in the presence of unstable accumulation. This can be overcome, for example, by constructing facies ''rank'' series, where exact facies thickness measurements can be made and preserved through high-resolution interpolation (see example in Section 3.1.3).

Empirical observation that stratigraphic accumulation rate estimates decrease over increasingly longer time scales raises the old question (Barrell 1917) of ''stratigraphic completeness'' (Sadler 1981, 1993, 1999). This occurs because lengthening the stratigraphic window increases the chances for capturing larger (rarer) hiatuses, greater compaction, etc. The data further indicate that the effect is strongest in nearshore facies and weakest in deeper-water facies—evidence that

the latter provide superior continuity over most stratigraphic time scales. Sadler (1994) also noted an anomaly in the trend in peritidal carbonate stratigraphy at the 10^4 year scale, which he interpreted as evidence for increased incidence of hiatuses at this time scale. Stratigraphic signals that contain hiatuses, depending on their durations and numbers, exhibit split spectral peaks (Weedon 1989). If the hiatuses are distributed non-randomly, as may be the case in many peritidal transgressive cycles—e.g. where discontinuities occur preferentially between supratidal mud-cracked laminites and overlying subtidal grainstones (e.g. Koerschner & Read 1989)—they are less likely to interfere with the time represented by the strata, and underlying time-periodic signals may still be legible (e.g. Bond et al 1991).

1.3.3 Autocycles vs. Allocycles Sedimentologists have long debated the origins of high-frequency stratigraphic cycles and have settled on two general concepts to explain them. The concept of autocyclicity recognizes that physical limits in certain sedimentary environments can result in repeated buildup, shutdown, and recovery of sedimentary accumulation over the long term, resulting in cyclic stratigraphy. Sedimentary facies that are prone to autocyclic depositional mechanisms include peritidal carbonates, turbidites, switching delta lobes, and tempestites (see review in Einsele et al 1991, pp. 5–13). In peritidal carbonates, a preferred time-periodic mode of stratigraphic cyclicity may develop without external cyclic forcing (Demicco 1998). This is because the peritidal environment can be filled in by lateral accumulation of sediment (progradation); the time it takes to fill the available platform or shelf to sea level will determine the value of this intrinsic time-periodicity. The lateral dimension of the depositional system is a major controlling factor of the periodicity, which is expected to overlap the orbital frequencies: For 40 km-wide shelves, autocycle periods are on the order of 20 kyrs, and for 100 km-wide platforms, 100 kyrs (Bazykin et al 1997, Bazykin 1997). It has also been demonstrated that a certain degree of self-organization in the stratigraphy of cyclic bedding thicknesses can be expected in the outcome (e.g. Drummond & Wilkinson 1993).

Allocyclicity refers to sedimentation that has responded to cyclically operating mechanisms external to the depositional system. Allocyclic stratigraphy should therefore reflect in some measure the cyclicity of the mechanism that forced it. If orbital forcing is involved, evidence for the presence of the multiple components that characterize orbital forcing would establish an allocyclic origin of the stratigraphy. When a depositional system is autocyclic and forced by allocyclic mechanisms, the output stratigraphy can become quite complicated—e.g. the increased turbidite recurrence in the Late Pleistocene Bahamian periplatform sequences in response to orbitally forced eustatic highstands vs. lowstands (Droxler & Schlager 1985).

1.3.4 Orbital Tuning Unstable accumulation, bioturbation, diagenesis, deformation, measurement error, and so on significantly distort and complicate the

recovery of orbital signals from stratigraphy. The removal of this stratigraphic noise, especially when the objective is to search for orbital signals, usually comes to involve some form of ''orbital tuning.'' Orbital tuning is the practice of aligning a stratigraphic signal thought to contain an orbital signal with a target orbital curve. The obvious problem with this practice is that power can be shifted from nearby uncorrelated frequencies into orbital frequencies (Neeman 1993, Shackleton et al 1995). Interpretations of orbitally tuned stratigraphy are thus always somewhat suspect. Judicious procedures can minimize the circular logic inherent to orbital tuning. It would be less objectionable, for example, to tune to one orbital parameter, e.g. obliquity; if a precession signal becomes aligned in the process, then orbital forcing can be argued as likely.

Other strategies develop time scales without fine-scale orbital tuning. The γ-method tests the hypothesis that different facies within stratigraphic cycles have unique accumulation rates, that their thicknesses are linearly related to times of development, and that the cycles were deposited on average over the same time period (Kominz & Bond 1990; see also Section 3.1). Accumulation rates for each facies are estimated by generalized linear inversion; these rates are used to develop an incremental time scale along the cyclic sequence. The crucial step in the process is deciding the time scale of the basic stratigraphic cycle, to make the final depth-to-time conversion. This usually involves testing to determine which of the orbital parameters scales to the basic stratigraphic cycle. Another technique compares amplitude and frequency modulations of stratigraphic cycle successions with those of orbital signals. Depth-to-time conversion is achieved indirectly by mapping the independent variables of the data (depth) and theoretical orbital signals (time) into a third independent variable that is common to both (cycle number). The superior capability of this procedure to suppress stratigraphic noise and uncover hidden signals is demonstrated in Section 2.3.4, Section 3.1, Section 3.4, and Section 3.5.

1.3.5 Sedimentological Tuning There is one underutilized sedimentological method for estimating high-frequency accumulation rates that is independent from a priori assumptions of orbital forcing. The method assumes that a specific sedimentary component—e.g. weight percent Al or TiO_2—accumulated at a constant rate. Therefore, fluctuations in its content along the section indicate dilution or concentration of the component from a variable influx of the remaining sediment. Early work on this method is summarized by Kominz et al (1979), who developed their own ''aluminum time scale'' for the Pleistocene V28–238 $\delta^{18}O$ record. This time scale significantly sharpened the data spectrum at the obliquity frequency, providing independent evidence for orbital control of $\delta^{18}O$ free from any starting assumption of orbital forcing. Similarly, Herterich & Sarnthein (1984) assumed that the accumulation rate of noncarbonate was constant in their Brunhes stratigraphy. Correcting the fluctuations of the concentration of noncarbonate along the series to a constant rate both increased spectral coherence in the obliquity and precession bands and resolved 23 and 19 kyr peaks within the precession band.

While there is little guarantee that any given sedimentary component accumulates at a truly constant rate, selecting one that represents a very small fraction of the total sediment influx, for which most of the variability in concentration is likely the consequence of fluctuations from the rest of the sediment, can do much to significantly advance the process of true time scale recovery. This should be explored wherever possible to free interpretations from the orbital tuning circularity problem.

1.3.6 Methods of Signal Analysis Numerous methods are now used in the time series analysis of stratigraphic and orbital signals (see recent review of well-known algorithms in Ghil & Taricco 1997). The most enduring and useful of these have been Fourier-based spectral estimators, although there are bias problems with some—e.g. the ever popular Blackman-Tukey estimator (Thomson 1990). Maximum entropy spectral analysis is not recommended (Kunzel 1989). Bispectral analysis has been used to assess nonlinear climatic signal responses to orbital forcing (e.g. Hagelberg et al 1991, King 1996). For signal cross-correlation studies, the spectral coherency estimator based on the Fourier transform remains the principal statistical tool (e.g. Pisias & Moore 1981, Thomson 1982).

Nonstationarity affects most long stratigraphic series, so time-frequency analysis (or evolutionary spectral analysis) is an important means for its characterization. It is used to detect amplitude and frequency variations resulting from changes in sedimentation and/or other primary responses to orbital forcing. Wavelet analysis has rapidly become a popular time-frequency method (e.g. Bolton et al 1995, Prokoph & Barthelmes 1996, Liu & Chao 1998). Empirical estimates for the probability distribution of wavelet power—hence the confidence limits and significance levels—can be made through Monte Carlo modeling (Torrence & Compo 1998). Other useful time-frequency methods include complex demodulation (e.g. Kominz et al 1979), envelope inversion (Park & Maasch 1993), complex signal analysis (e.g. Liu 1995; see also Section 2.3.1), and cycle modulation analysis (see Section 2.3).

''Signal'' in the context of orbital forcing is premised on the presence of one or more sinusoidal frequencies that arise from persistent autocorrelation of the forcing process through time. Evaluation of the presence and significance of these process frequencies is accomplished through harmonic or power spectral analysis; statistical significance is determined by hypothesis testing against alternative ''noise'' models of the series. Traditionally, this has been done by comparing the lower 99% or 95% confidence limit of the estimated spectral power of the series to the power of an equivalent ''white'' (i.e. uncorrelated at all frequencies) or ''red'' (i.e. partially correlated at the lowest frequencies) noise spectral model estimated from the autocorrelation lags 0 and 1 of the series (e.g. Jenkins & Watts 1968). However, these models overestimate the true noise of the series because they retain all of the signal as well as the noise. To minimize this bias, Mann & Lees (1996) developed a procedure of fitting a red noise model to a median-smoothed background estimate of the series spectrum. This ''robust'' approach

suppresses anomalously large contributions from high-power, narrow-band (or single-frequency) components in the series spectrum that clearly constitute signal. This bias problem implies that a lot of past work that relied on the traditional autoregressive models may have rejected significant spectra.

2. THEORY: ORBITALLY FORCED SOLAR RADIATION

2.1 Status of the Theory of Earth's Orbital Parameters

2.1.1 Overview The theory addressing the general problem of planetary motion has recently been revised and improved through the introduction of new numerical techniques, the inclusion of new high order terms, and the incorporation of lunar and relativistic effects in the computation of orbital elements. The chief motivation in developing a new planetary solution was for exploration of the long-term stability of the Solar System, long suspected to be chaotic (Peterson 1993). The new solution for Earth's orbital parameters has proved to be a highly precise template for evaluating the connection between orbitally forced incoming solar radiation (insolation) and Earth's climatic responses, especially in the high-resolution calibration of Late Cenozoic stratigraphy. Finally, Earth's rotational history and Earth-Moon dynamics through time have been shown to have a significant effect on Earth's precession rate and obliquity (Berger et al 1989, 1992; Berger & Loutre 1994). Consequently, today's orbital models now explicitly define parameters for the effects of tidal dissipation and Earth's dynamical ellipticity (see Section 2.1.3).

2.1.2 The Orbital Elements Knowledge of the planetary motions and orbits forms the basis for estimating the Earth's orbital parameters that affect insolation. Two complex variables, z and ζ, are used to describe orbital motion; each encapsulates two fundamental orbital elements: (*a*) orbital eccentricity (e) and longitude of perihelion (Π), $z = e\,exp[i\Pi]$; and (*b*) orbital inclination (I) and longitude of the ascending node (Ω), $\zeta = sin(I/2)\,exp[i\Omega]$, where $i = (\sqrt{-1})$. Traditionally, z and ζ are expressed as Poisson series with fundamental contributions from each of the eight planets; the series for the Earth are summarized in Table 1. A full description of the orbital elements and the origin and determination of the series arguments appears in Berger & Loutre (1990, 1991).

Early orbital models were valid to only a few million years b.p. (e.g. Berger & Loutre 1991). It was not until sensitivity experiments and an analysis of the uncertainties in the initial conditions were conducted that specific limits were placed on the model's time validity (Laskar 1999). Presently, Laskar's full orbital model is accurate to about 16 million years b.p.; the limiting source of uncertainty originates from the current state of knowledge of the oblateness of the Sun. If this uncertainty can be reduced by 2 orders of magnitude from its current value, then the validity of the orbital model can be extended to 30–35 million years b.p.

TABLE 1 Earth's fundamental amplitude, frequency, and phase terms[a]

A. $z = (h,k) = e \cdot \exp[i\Pi] = \sum_{j=1}^{20} A_j \exp[i(\nu_j t + \beta_j)]$

j	composition of ν_j	$A_j \times 10^6$	ν_j (″/yr)	β_j (degrees)
1	g_5	18913	4.2487910	30.597
2	g_2	16047	7.4559199	200.630
3	g_4	13159	17.9155811	155.568
4	g_3	9406	17.3646123	304.902
5	g_1	4248	5.5964883	112.565
6	$g_3 - \theta$	2238	17.0830020	351.000
7	$g_3 + \theta$	1956	17.6287061	7.770
8	$g_3 - 2\theta$	1722	16.8132568	94.866
	$2g_3 - g_4$			
	$g_4 + g_3 - s_4$			
9	unknown	1598	6.9349219	169.028
10	g_6	1506	28.22066002	128.008

B. $\zeta = (p,q) = \sin(I/2)\exp[i\Omega] = \sum_{j=1}^{20} A_j \exp[i(\nu_j t + \beta_j)]$

1	s_5	13773	0.0000000	107.586
2	s_3	8760	−18.8511680	240.034
3	s_1	4960	−5.6176875	348.307
4	s_4	4024	−17.7482549	303.928
5	s_2	3431	−7.0797568	93.267
6	$s_3 + 2\sigma$	2846	−18.2999619	270.439
	$s_3 - g_3 + g_4$			
	$s_4 + g_3 - g_4$			
7	$s_2 + 2\sigma$	1736	−6.8410195	286.932
8	$s_2 + \sigma$	1736	−6.9609463	277.682
9	$s_2 - \sigma$	1610	−7.1949375	285.060
10	$s_3 - 2\theta$	1607	−19.4022773	29.348
	$s_3 + g_3 - g_4$			

[a]For (A) orbital eccentricity and longitude of perihelion variable z, and (B) orbital inclination and longitude of node variable ζ (from Laskar 1990, Tables II and III, results of a 20 Myr analysis). The first 10 terms are listed out of a total of the 20 that were computed for the Earth. Fundamental secular frequencies g_m and s_m identify orbital eccentricity and inclination contributions, respectively, from the eight planets, where $m = 1$ refers to Mercury, $m = 2$ to Venus, etc. The terms $\theta = 0.28''/yr$ and $\sigma = 0.12''/yr$ are libration frequencies identified with important secular resonances involving Earth-Mars and Mercury-Venus-Jupiter orbital interactions (Laskar 1990). N.B.: In earlier publications (e.g. Bretagnon 1974, 1984; Berger 1977) Earth's fundamental frequencies were designated g_j; Laskar instead specified the planetary origins of the frequencies, and so reassigned them as ν_j, and identified the composition of ν_j in terms of g_m and s_m.

Secular frequencies of the (slightly) more stable outer planets may provide specific orbital modes that are valid over much longer time scales. The most promising of these mentioned by Laskar (1999) are g_2 and g_5, where $g_2 - g_5$ appears as the dominant 404 kyr component of the Earth's orbital eccentricity (see Section 2.1.3), where g_5 was determined to be nearly constant over the past 200 Myrs (Laskar 1990, his Figure 8). However, recognition of this mode in stratigraphy from very remote geological times may be problematic. This is because geological evolution of the precession index, which carries the eccentricity mode in the insolation variations, also depends on the evolution of k (see Section 2.1.4 and Section 3.5).

2.1.3 Earth's Orbital Parameters The fundamental frequencies g_m and s_m of the secular planetary system appear in the solution for Earth's orbital eccentricity (e), obliquity (ε), and precession index ($e\sin\varpi$) (Table 2). Although only the first few highest amplitude terms are listed, the full perturbation series solution, for example, in Berger & Loutre (1991) for e has 11,479 terms, ε has 6480 terms, and $e\sin\varpi$ has 12,880 terms. Laskar et al (1993), however, indicate that since the orbital solution is not truly quasiperiodic, trigonometric approximations should be avoided, and numerical integrations should be performed for highest accuracy. For this purpose, FORTRAN routines may be downloaded from Laskar's Internet site at ftp://ftp.bdl.fr/pub/ephem/sun/la93. The nominal solution La93(0,1) is given; other solutions, such as La93(CMAR, FGAM), where CMAR is the input for the tidal effect of the Moon and FGAM is the input for the dynamical ellipticity of the Earth, are computed from this nominal one.

A plot of the three orbital parameters and their spectra for the past 10 million years appears in Figure 1. All three parameters exhibit clusters of ''multiplets'' that attest to their complicated origins (cf Table 2). Within this particular 10-Myr observation window, these components modulate in frequency and in amplitude; thus, they have unique phasing properties that are an important key to unravelling climatic responses to orbital forcing (Berger et al 1998). The relationships among these modulations allow for the development of additional correlation tests that can be used to link orbital signals and stratigraphic data. These topics are explored more fully in Section 2.3 and Section 3.4.

2.1.4 Orbital Parameters Through Time The Earth's precession rate k plays a central role in the obliquity and precession index. It appears as a constant of integration in the solution for Earth's general precession in longitude (see e.g. Berger & Loutre 1991). Its computed value thus depends on the model assumed for the general precession, the initial conditions, and the limits of integration in the model solution. This explains the different values of k that appear in the literature, e.g. 50.″439273/yr (Berger 1978a), 50.″417262/yr (Berger & Loutre 1991, denoted as k), and 50.″4712/yr (Laskar et al 1993, denoted as p). Also, k is dependent on the Earth's rotation rate, dynamical ellipticity, and the Earth-

TABLE 2 Principal terms for Earth's orbital parameters[a]

A. Eccentricity: $e = e_0 + \sum_{n=1}^{N_e} E_n \cos(\lambda_n t + \phi_n)$

n	E_n	λ_n (″/yr)	ϕ_n (degrees)	period (yr)	origin of λ_n (″/yr)
1	0.010851	3.1906	168.02	406193	$g_2 - g_5$
2	0.009208	13.6665	121.71	94830	$g_4 - g_5$
3	0.007078	10.4615	–36.79	123882	$g_4 - g_2$
4	0.005925	13.1430	–86.17	98607	$g_3 - g_5$
5	0.005295	9.9677	115.55	130019	$g_3 - g_2$
etc	:	:	:	:	: :

B. Obliquity: $\varepsilon = \varepsilon^* + \sum_{n=1}^{N_\varepsilon} A_n \cos(f_n t + \delta_n)$, $\varepsilon^* = 0.4006657$, $k = 50.4576$ ″/yr

n	A_n	f_n (″/yr)	δ_n (degrees)	period (yr)	origin of f_n (″/yr)
1	0.011168	31.6132	86.26	40996	$k + s_3$
2	0.004401	32.6799	89.28	39657	$k + s_4$
3	0.003010	32.1827	103.74	40270	$k + s_3 + g_4 - g_3$
4	0.002912	24.1277	–46.03	53714	$k + s_6$
5	0.002625	31.0981	117.31	41674	$k + s_3 - g_4 + g_3$
6	0.001452	44.8609	–175.78	28889	$k + s_1$
etc	:	:	:	:	:

C. Precession index: $e \sin \omega = \sum_{n=1}^{N_p} P_n \sin(\alpha_n t + \psi_n)$, $k = 50.4576$ ″/yr

n	P_n	α_n (″/yr)	ψ_n (degrees)	period (yr)	origin of α_n (″/yr)
1	0.018839	54.7064	–52.51	23690	$k + g_5$
2	0.016981	57.8949	113.26	22385	$k + g_2$
3	0.014792	68.3691	71.29	18956	$k + g_4$
4	0.010121	67.8626	–131.00	19097	$k + g_3$
5	0.004252	56.0707	–3.96	23114	$k + g_1$
etc	:	:	:	:	:

[a]From a 4 Myr analysis in Laskar 1999. Only the first few terms are listed. Berger & Loutre (1990) give a full mathematical account for the origin of the modes λ_n, f_n, and α_n, summarized here in Column 6 of each table, where g_m and s_m are the fundamental secular frequencies as in Table 1. Values for g_m and s_m differ slightly from those given in Table 1 as a result of the shorter 4 Myr analysis.

Moon distance, all of which are thought to have varied significantly through geologic time (Berger et al 1992; see also stratigraphic evidence in Section 3.5). Table 3 gives one estimate by Berger & Loutre (1994) of the long-term evolution of k for the past billion years, indicating significant increases and consequently a shortening effect on the principal modes of the obliquity and precession index.

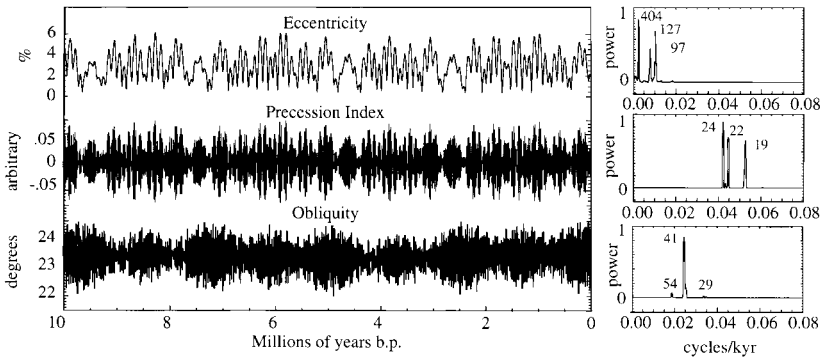

Figure 1 Earth's orbital parameters over the past 10 Myrs calculated using Analyseries (Paillard et al 1996) and the La90(0,1) solution. The time series are displayed on the left panel; 4π multi-tapered power spectra (Thomson 1982) are on the panels to the right. The labeled peaks identify periodicity in kyrs. Note that the spectral averaging does not reveal that most of the peaks displayed are composed of several harmonic components, e.g. in the eccentricity spectrum; the depicted 127 kyr peak is composed of two components at 124 kyr and 130 kyr (cf Table 2A).

Thomson (1991) detected an apparent shorter-term decrease in k in the Late Pleistocene $\delta^{18}O$ record that was attributed to an ellipticity response of the Earth to large ice sheets in the Northern Hemisphere.

Long-term changes in k might be detected in stratigraphy by examining the frequency ratios between measured obliquity and precession index frequencies and those of the more stable eccentricity. Faster k in remote geological times would translate into higher ratios of eccentricity vs. obliquity or eccentricity vs. precession index frequencies, as well as obliquity vs. precession index frequencies, as long as the perturbing secular frequencies g_m and s_m remained stable (see examples of stratigraphic evidence in Section 3.5).

2.2 Orbitally Forced Solar Radiation on Earth

2.2.1 The Insolation Equation The equation describing the *instantaneous insolation* on a horizontal surface at any geographical point on Earth is (e.g. Berger et al 1993):

$$W = S\,\rho^{-2}\,\cos Z, \tag{1}$$

where $S = S_0(1\text{-}e^2)^{0.5}$; S_0 is the solar constant, e is Earth's orbital eccentricity, and the normalized Earth-Sun distance $\rho = r/a$, where r is the Earth-Sun distance and a is the semi-major axis of the Earth's orbit. The vertical component of the insolation relative to the Earth's surface is defined by:

TABLE 3 Schematic model of changes in the periods of the principal modes of (A) Earth's obliquity variation and (B) Earth's precession index.[a]

A. Change in principal modes f_n of the Earth's obliquity

Time (Myr B.P.)	k (′/yr)	f_1^{-1} (yrs)	f_2^{-1} (yrs)	f_3^{-1} (yrs)	f_4^{-1} (yrs)	f_5^{-1} (yrs)	f_6^{-1} (yrs)
0.0000	50.431631	41057	39663	40353	53805	41786	28929
72.000	51.800236	39333	38052	38687	50883	40002	28062
270.00	56.070946	34820	33812	34312	43577	35343	25687
298.00	56.742065	34203	33231	33713	42615	34708	25350
380.00	58.818901	32426	31550	31985	39891	32879	24360
440.00	60.432739	31168	30358	30760	38003	31586	23643
500.00	62.173118	29916	29169	29540	36158	30301	22916
1000.0	69.585861	25545	29498	25270	29961	25825	20260

B. Change in principal modes α_n of the Earth's precession index

Time (Myr B.P.)	k (″/yr)	α_1^{-1} (yrs)	α_2^{-1} (yrs)	α_3^{-1} (yrs)	α_4^{-1} (yrs)	α_5^{-1} (yrs)
0.0000	50.431631	23708	22394	18966	19120	23137
72.000	51.800236	23123	21871	18590	18738	22580
270.00	56.070946	21485	20401	17517	17648	21016
298.00	56.742065	21249	20188	17359	17488	20790
380.00	58.818901	20549	19555	16889	17012	20119
440.00	60.432739	20037	19090	16542	16659	19628
500.00	62.173118	19512	18613	16182	16294	19124
1000.0	69.585861	17553	16822	14811	14905	17238

[a]These simplified estimates were computed using Column 6 of Table 2B and 2C, g_m and s_m from Table 1, and the value of k through geologic time, which takes into account the variation of Earth-Moon distance, change in length of day, and Earth's dynamical ellipticity (Berger & Loutre 1994, their Table 2, Model 2).

$$\cos Z = \sin\phi\sin\partial + \cos\phi\cos\partial\cos H, \quad (2)$$

where at geographical latitude ϕ the Sun in the local sky is at angle Z from zenith at hour angle H; ∂ is the Sun's declination, the angle between the Sun and the Celestial Equator along the meridian.

The Sun's declination ∂ varies during the Earth's annual orbital circuit, i.e. over the Earth's true longitude λ in the heliocentric reference frame, according to $\sin\partial = \sin\lambda\sin\varepsilon$. ∂ also depends on ε, so Equation 2 varies interannually with the Earth's obliquity.

The normalized Earth-Sun distance in W appears as:

$$\rho^{-2} = [1 + e\cos(\lambda - \tilde{\omega})]^2/(1 - e^2)^2, \quad (3)$$

where λ is Earth's true (heliocentric) longitude as above, and ϖ is the moving longitude of perihelion. Thus the precession index variation occurs in W with a phasing set by λ and ϕ. Consequently, the variation is not strictly $e\sin\varpi$ at all times and locations. In the tropics, $|\phi| < \partial$, and the Sun passes through minima in Z twice a year; this results in two insolation maxima per annum. If climate responds to both maxima, the result over the long term will be a half-precession response (Berger & Loutre 1997).

The contribution from eccentricity e to W averaged over a year is $(1\text{-}e^2)^{-0.5}$; for Earth's orbital eccentricity values over [0.005, 0.060] this represents changes on the order of 10^{-3} or less in the total insolation. This small theoretical contribution has caused considerable difficulty in connecting W to major ~100 kyr variations commonly observed in cyclic stratigraphy (e.g. Imbrie et al 1993). However, e is also present as a modulator in the precession index, which appears to account for much of the variability in paleoclimatic responses to W.

2.2.2 Rubincam's Insolation Rubincam (1994) proposed an alternative formulation of W based on a spherical harmonic expansion of Equation 2 in a geocentric reference frame, after Kaula (1966). Adapting the above notation of W to Rubincam's Equation 6 gives:

$$\begin{aligned} W &= S_0\left(\frac{r_0}{a}\right)^2 \\ &\cdot\sum_{l=0}^{\infty} d_l \sum_{m=0}^{l} (2-\delta_{o,m})\frac{(l-m)!}{(l+m)!}P_{l,m}(\sin\phi) \\ &\cdot\sum_{p=0}^{l}\sum_{q=-\infty}^{+\infty} F_{l,m,p}(\varepsilon)w_{l-2p,q}(e) \\ &\cdot\begin{bmatrix}\cos\\ \sin\end{bmatrix}_{l-m,odd}^{l-m,even}[(l-2p)\omega + (l-2p+q)M + m(\Omega - H - \Lambda)], \end{aligned} \quad (4)$$

where r_0 is a reference Earth-Sun distance, ω is the argument of perigee ($\omega = \tilde{\omega} + 180°$), ϕ, Λ are terrestrial latitude and longitude, and Ω is the longitude of the ascending node of the Sun. The coefficients d_l are given in Rubincam (1994, Table 1); the $P_{l,m}(\sin\phi)$ are associated Legendre functions; $F_{l,m,p}(\varepsilon)$ are inclination functions used in geodetic applications, given in Rubincam (1994, Table 2); $w_{l\text{-}2p,q}(e)$ are modified eccentricity functions, given in Rubincam [1994, Table 3; Rubincam (personal communication) notes that for ($l\text{–}2p = +1$, $q = +1$) and ($l\text{–}2p = -1$, $q = -1$), the term e^4 should be e^3]. Although cumbersome in its derivation, Equation 4 is easy to use to calculate diurnal (H), seasonal (M), and longer-term insolation time series at any geographical location ϕ, Λ. Discontinuities in the classical insolation equation at latitudes experiencing polar night (e.g. Berger 1978a) are fully absorbed in the expansion; reference to the Sun's declination ∂

appears in the argument ε. The only difference between Equation 4 and Equation 1 is that Equation 4 uses *M* (mean anomaly) in the place of true longitude λ. (The relation between *M* and λ is given in Berger 1978b).

Equation 4 shows that *W* contains high frequency components involving *H* and *M*; the argument ω acts to modulate these frequencies, which prompted Rubincam to clarify the role played by the precession index in the insolation variations. This led to a controversy (Berger 1996, Rubincam 1996) in which Berger maintained that the precession index is intrinsic to insolation and observable when computing *W* at specific times—i.e. sampling insolation for selected values of *H* and *M*. Rubincam argued that selective sampling of *W* was tantamount to assuming a climate model, and was a manipulation of the high-frequency insolation signal to obtain kyr periods. In light of the widespread presence of precession index-like variations in the stratigraphic record, $e\sin\varpi$ remains meaningful as a generic indicator of interannual seasonal insolation. At the same time, it is important to recognize that precession index-like variations arise only in filtered outputs of orbitally forced insolation, and that to fully understand the insolation response by Earth's climate requires first and foremost an appreciation of the fundamental high-frequency nature of *W*. Therefore, *W* that is sampled interannually, integrated, or otherwise filtered, will be referred to as $\overline{W}$.

2.2.3 Earth's Insolation Response The relative contributions of the obliquity and precession index in insolation that come to affect Earth's climate depend on time(s) of year, geographical latitude, and the Sun's elevation (time of day). Basic scenarios exploring these factors were analyzed by Cerveny (1991) and again by Berger et al (1993), who concluded that variations in $\overline{W}$ are dominated by the precession index, although high latitudes experiencing conditions of perpetual day or night during non-equinoctial times also have a strong obliquity component. For a given ''local'' season, these precession-dominated insolation signals are out of phase between the Northern and Southern Hemispheres. On the other hand, at the solstices, insolation that occurs at high solar elevations (low *Z*)—e.g. to which ice surfaces are most sensitive—reveals that *W* that is time-integrated over near-noon values of *Z* has a dominant obliquity component at all latitudes. As noted by Cerveny (1991), this ''solar noon elevation angle class'' or ''noon zenith-class'' (Berger et al 1993) amplification of the obliquity, which is in phase between the Northern and Southern Hemispheres, could explain the interhemispheric synchroneity of the last deglaciation (Broecker & Denton 1989, Lowell et al 1995); this synchronous deglaciation cannot be explained by the daily, precession-dominated (i.e. anti-phased) summer insolation. The surface integrations of insolation in the energy balance models of Short et al (1991) further underscore the range of potential climatic responses to insolation at orbital scales that are possible, and also explain the climatic transfer of orbital power from the precession index into the eccentricity (producing the famous 100 kyr variations commonly observed in the stratigraphic record) and half-precession bands in the intertropical zone.

2.3 The Emerging Significance of Orbital Signal Modulations

2.3.1 Background Over 50 years ago, in a study of the Lofer cyclothems of the Late Triassic Dachstein Formation (Northern Calcareous Alps), Schwarzacher (1947) observed that the meter-scale cyclothem thicknesses were bundled in a 5:1 stratigraphic pattern. Facies analysis of the cyclothems suggested that eustatic oscillations had caused cyclothem formation; geochronology indicated an average cyclothem formation time of 21.1 kyr (Fischer 1964). These facts established the basis for interpretation of the Lofer succession as a depositional response to repeated sea level oscillations under orbital control (Schwarzacher 1993). Subsequently, there have been numerous reports of similar 5:1 cycle bundling patterns, primarily in other Mesozoic carbonates (Fischer 1991); it is now widely believed that the cycles were generated by mechanisms driven by the precession index $esin\varpi$, and that the bundles were modulations originating from the 100-kyr component of the eccentricity modulator *e*. Schwarzacher & Fischer (1982) discovered a second, lower frequency indicating a 20:1 bundling pattern superimposed on the 5:1 bundles in the cycles of the Lower Cretaceous Maiolica Limestone (Italy); this was interpreted as evidence for the 400 kyr component of the eccentricity modulator. Herbert (1992) considered the more complete hypothesis that the variable Maiolica cycle thicknesses were related to the modulating durations and/or amplitudes of precession index cycles, thereby leading cyclic stratigraphy and the analysis of orbital signals into a new quantitative field—namely, amplitude modulation (AM) and frequency modulation (FM) analysis.

In an independent application, Liu (1995, 1998) used complex signal analysis, a classical technique in the study of nonstationary time series (e.g. Gabor 1946, Bracewell 1965, Rowe 1965), to study the frequency variation (or frequency modulation) of Earth's obliquity parameter. The technique treats the real orbital signal *f(t)* as the complex variable:

$$F(t) = f(t) + if^*(t) = A(t)\,\exp[i\theta(t)], \tag{5}$$

where the quadrature signal *f*(t)* is obtained by Hilbert transformation of *f(t)* (see Taner et al 1979 for processing information). The amplitude modulation of the signal is thus:

$$A(t) = [f^2(t) + f^{*2}(t)]^{0.5} \tag{6}$$

and its frequency modulation is:

$$\eta(t) = \frac{d\theta(t)}{dt} = \frac{f(t)\,\frac{d}{dt}\,f^*(t) - f^*(t)\,\frac{d}{dt}\,f(t)}{f^2(t) + f^{*2}(t)}. \tag{7}$$

Equations 6 and 7 may be used to calculate the amplitude and frequency modulation series of the precession index and obliquity, such as those shown in Figures

2 and 3. Liu observed that the frequency modulation of the obliquity has a major 100 kyr periodicity, which he suspects is a major player in the Late Pleistocene glaciations (Liu 1998; Section 3.3).

2.3.2 Modulations of the Precession Index The precession index (Figure 1*a*) tracks the normalized Sun-Earth distance as the equinoxes precess around the Earth's (revolving) eccentric orbit. As discussed in Section 2.2.1, the index appears in W as ρ^{-2}, where it has an average value of 1 and ranges between [0.9,1.1] (Berger et al 1993, their Figure 3). The index thus experiences modulations from the orbital eccentricity e in both amplitude and frequency, as shown in AM and FM series calculated from $e\sin\varpi$ for the past 10 million years (Figure 2*a*). The power spectra of these series (Figure 2*b*) exhibit the principal modes of the eccentricity, with the curious exception of the 97 kyr component in the FM spectrum, which is greatly suppressed. (This is the 100 kyr spectral ''hole'' described in Herbert 1992, p. 25). The components centered at 404 kyr, 127 kyr, and 97 kyr are directly associated with the first five eccentricity components (cf Table 2A). The low power components at 2.5 Myr, 1.0 Myr, and 670 kyr are related to the $g_4 - g_3$, $g_1 - g_5$, and $g_1 - g_2$ contributions to the eccentricity (Olsen & Kent 1999, their Table 3).The component at 204 kyr is a transient signal that appears during times when the 404 kyr and 19 kyr components pass through maxima (Figure 2*a*, vertical arrows labeled ''204''). The components at 77 kyr and 63 kyr likewise arise as transients when the 404 kyr and 19 kyr components are at a minimum (Figure 2*a*, vertical arrows labeled ''77''). These transient components can also be seen in Berger et al (1998, their Figure 3). The relationship between the AM and FM components is fully revealed using spectral coherency analysis. The aforementioned components are all highly coherent between the AM and FM series, but the cross-phase spectrum reveals some surprises (Figure 2*c*): the 404 kyr and 204 kyr AM and FM components are in phase (0°), but the 127 kyr and 97 kyr components are 180° out of phase, as are the components at 2.5 Myr. In other words, at these frequencies, when precession cycle amplitudes are relatively high, their periods are relatively short, and vice versa.

2.3.3 Modulations of the Obliquity The AM and FM series of the obliquity appear in Figure 3*a*. The modulation patterns are quite dissimilar to those of the precession index (cf Figure 2*a*) owing to their largely separate origins: The precession index modulations are caused by perturbations in k from the secular frequencies g_m, whereas the obliquity modulations originate from perturbations in k from s_m (see Tables 2B and 2C). The obliquity modulations, unlike the eccentricity modulations of the precession index, cannot be related to a single physical mechanism. Thus, the AM and FM obliquity series record ''beat'' frequencies (i.e. difference tones) produced by the s_m. The power spectra (Figure 3*b*) exhibit a suite of modulation frequencies that is clearly distinguishable from that of the precession modulations (cf Figure 2*b*). Again, the relative power of the components differs between the AM and FM spectra. The coherency and cross-phase

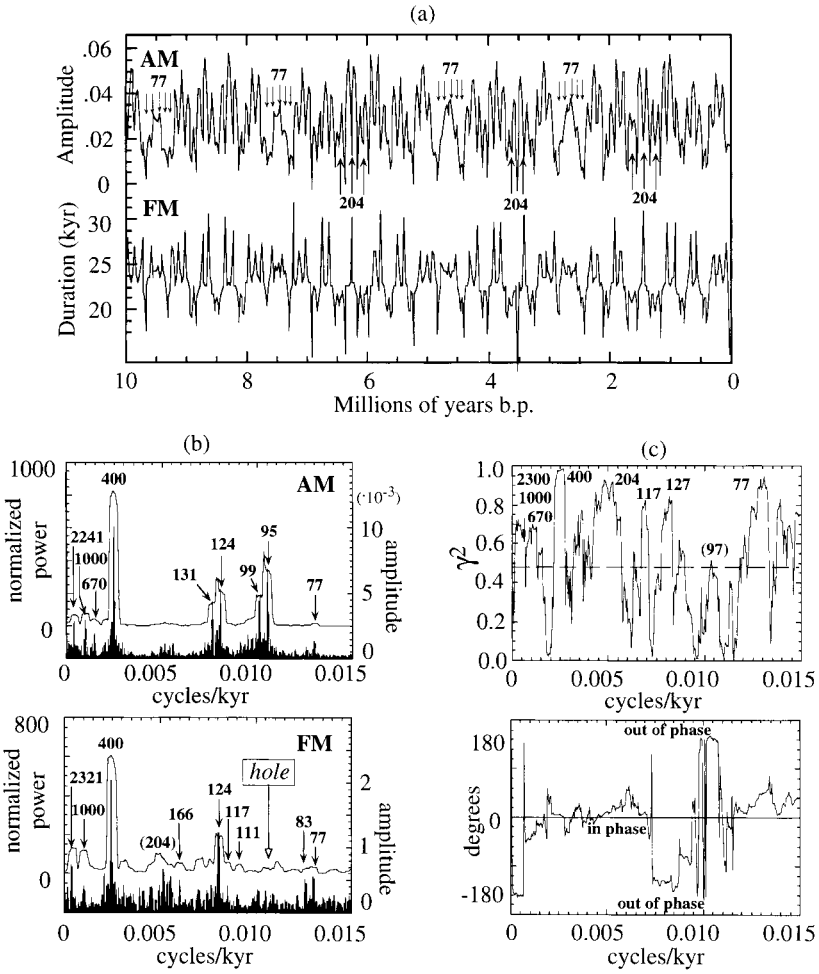

Figure 2 Amplitude and frequency modulations of the precession index signal depicted in Figure 1. (*a*) The AM series records the peak amplitudes of successive precession cycles and records the results at the times at which the peak amplitudes occur. The FM series measures durations between cycle maxima, and records the result at a time halfway between the maxima. The arrows labeled ''204'' and ''77'' refer to intermittent power contributions to the averaged spectra (see text). (*b*) 4π multi-tapered power spectra of the AM and FM series (power axis on the left). Also shown are the results of a 4π multi-taper harmonic analysis (amplitude axis on the right); labeled components are in kyrs and identify harmonic components that passed F-tests at the 99.5% significance level (except those in parentheses). (*c*) 4π multi-tapered squared-coherency and cross-phase spectral analysis of the AM vs. FM series. The estimates have an average of at least 12 degrees of freedom, for which the 95% significance level for true zero coherence is 0.394 (after Priestley 1981).

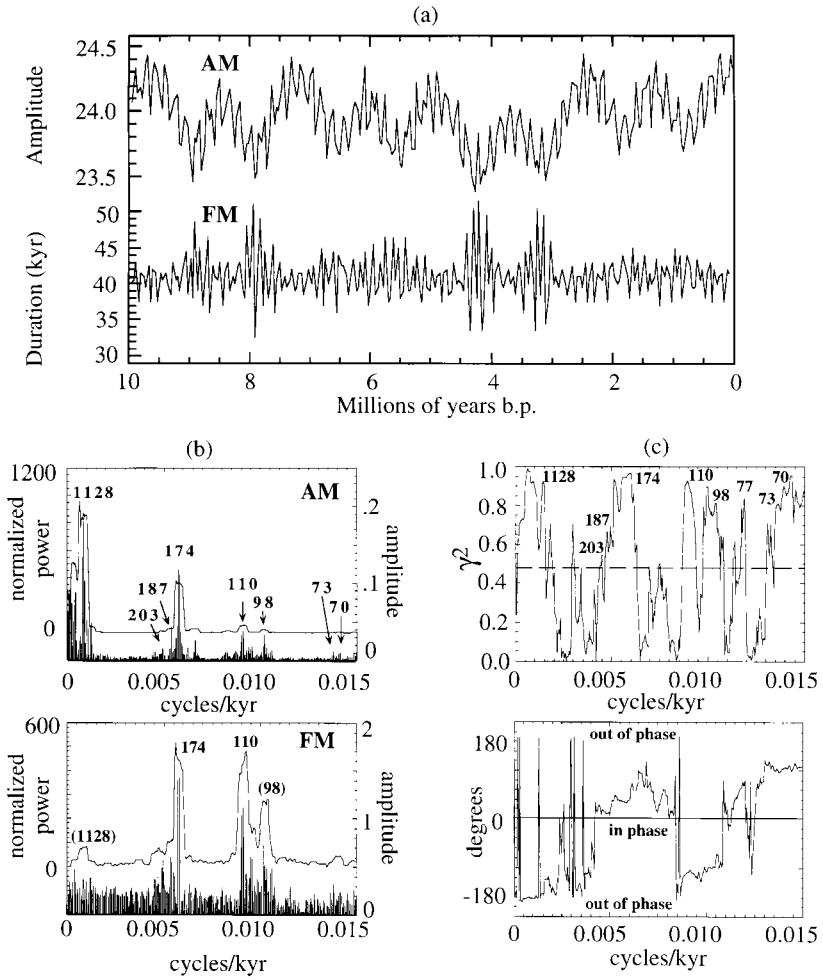

Figure 3 Amplitude and frequency modulations of the obliquity signal depicted in Figure 1. All labels identify periodicity in kyrs (those in parentheses do not pass the 99.5% significance level). (*a*), (*b*) and (*c*) are otherwise as in Figure 2.

spectra (Figure 3*c*) show a somewhat complicated relationship between the amplitude and frequency modulations: The 174 kyr components are phase shifted, with cycle period increases leading cycle amplitude increases by 45°, i.e. ~174 kyr/8 = 22 kyr, or by half an obliquity cycle. The 110 kyr and 98 kyr components register a cross phase of about 90°—i.e. cycle amplitude increases lead cycle duration increases, also by half an obliquity cycle. The 1.1 Myr AM and FM components are 180° out of phase.

2.3.4 Stratigraphic vs. Metronomic Analysis Cycle modulation analysis is best suited for stratigraphic sections with hundreds of cycles that span millions of years. For example, identification of the important 404 kyr modulation of the precession index requires a time span of at least 808 kyrs (two completions of the cycle). At the same time, over such long time intervals, accumulation rates are prone to vary substantially; the reconstruction of AM and FM signals from such stratigraphy will suffer the same distortions as all other stratigraphic series. To illustrate, Figure 4*a* shows the AM series resulting from a 10 Myr-long precession series that has been transformed into two stratigraphic sections—one has accumulated at a constant rate of 1 cm/kyr, for a stratigraphic section 100 meters thick (Series A), and the other has accumulated with rates increasing from 1 cm/kyr to 2 cm/kyr over the same 10 Myr period, yielding a section nearly 200 meters thick (Series B). The Series A spectrum, now with a frequency scale in cycles/cm, is otherwise identical to that in Figure 2*b.* The spectrum of Series B, however, shows a dramatic distortion and mixing of modes that have resulted from the stretching of the cycles with accelerated accumulation. The effect on the FM series (Figure 4*b*) is similar in shifting the principal FM modes to lower frequencies; in addition, the thicknesses and the variations in thicknesses increase in amplitude up the section (this is registered as higher power, i.e. variance, in the FM spectrum of Series B).

These problems are minimized when the AM and FM modulation series are instead recorded as a function of cycle number (Figure 5). This ''metronomic'' (Herbert 1994) representation of stratigraphic cycle modulations is directly comparable to metronomic AM and FM compilations of the orbital parameters because they now share the same independent variable (cycle number). The AM Series A and B and their spectra (Figure 5*a*) now are identical; effects from the accumulation rate change have been removed entirely by the cycle number scale. Similarly, the FM Series A and B show stable spectra (Figure 5*b*); the only difference is in the increased power in the Series B spectrum (from increasing thicknesses and thickness variations upsection). Figure 6 and Table 4 identify the principal metronomic AM and FM frequency components of the precession index and obliquity. It should be noted that over different time windows and window lengths, the relative power of these modulation components can vary significantly, as can their frequencies (see Hinnov & Park 1998 for examples).

In many respects, metronomic AM/FM analysis parallels the philosophy of orbital tuning. Orbital tuning assumes that an orbital signal is present in the data, and within the limits of the geochronologic controls, the data is adjusted until its correlation with respect to a (somewhat arbitrarily chosen) target orbital curve is maximized (e.g. Martinson et al 1982, Brüggemann 1992). This correlation then becomes the basis for interpretation of the data. Metronomic analysis sets up AM/FM models of orbital parameters with respect to an independent variable based on cycle number, and compares the models to stratigraphic data recorded also as a function of cycle number. No further steps are taken to adjust the data relative to this independent variable; in this way, metronomic analysis differs fundamen-

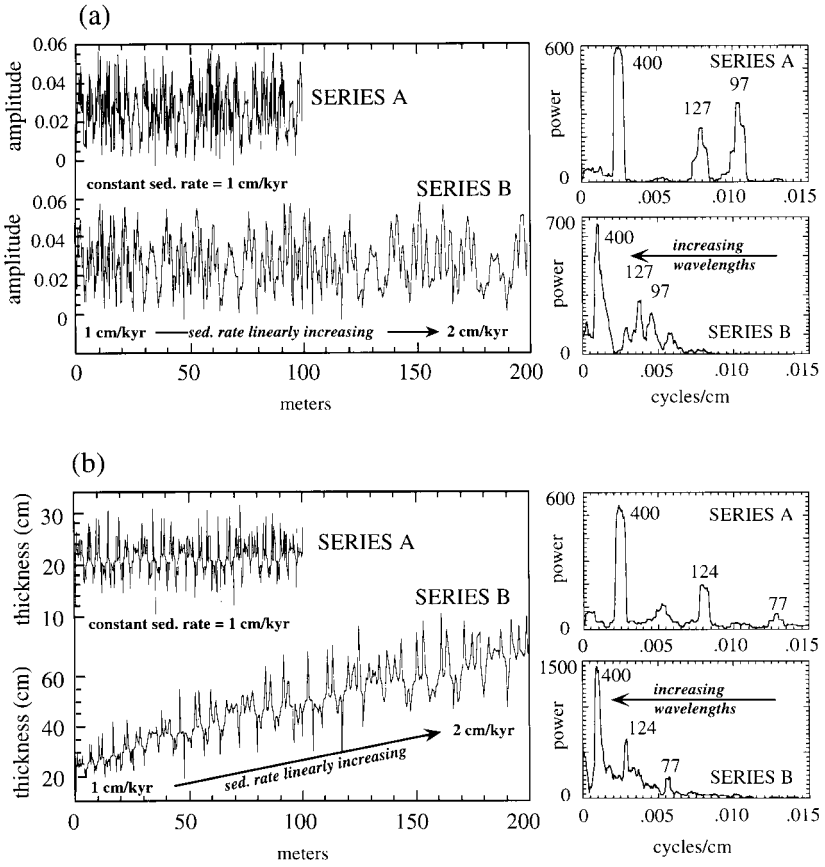

Figure 4 Stratigraphic measurement of 10 Myrs of two modeled precession index-forced (after Figure 1) stratigraphic series: one that accumulated at a constant rate, and the other with a monotonically increasing rate. (*a*) *Left panel:* amplitude modulations (AM) recorded as a function of stratigraphic position (in meters) of a stratigraphic model accumulating at 1 cm/kyr (SERIES A), and of a model subjected to accumulation accelerating from 1 to 2 cm/kyr (SERIES B); *Right panels:* 4π multi-tapered AM power spectra of SERIES A and B, showing frequency distortion in the SERIES B spectrum as a result of the progressive shift in the series to thicker cycles (longer wavelengths). (*b*) *Left panel:* frequency modulations (FM) of SERIES A and B, recorded as in (*a*); *Right panels*: 4π multi-tapered FM power spectra of SERIES A and B, showing frequency distortion and increased power in the SERIES B spectrum as a combined result of the progressive shift in the series to thicker cycle and greater thickness variations.

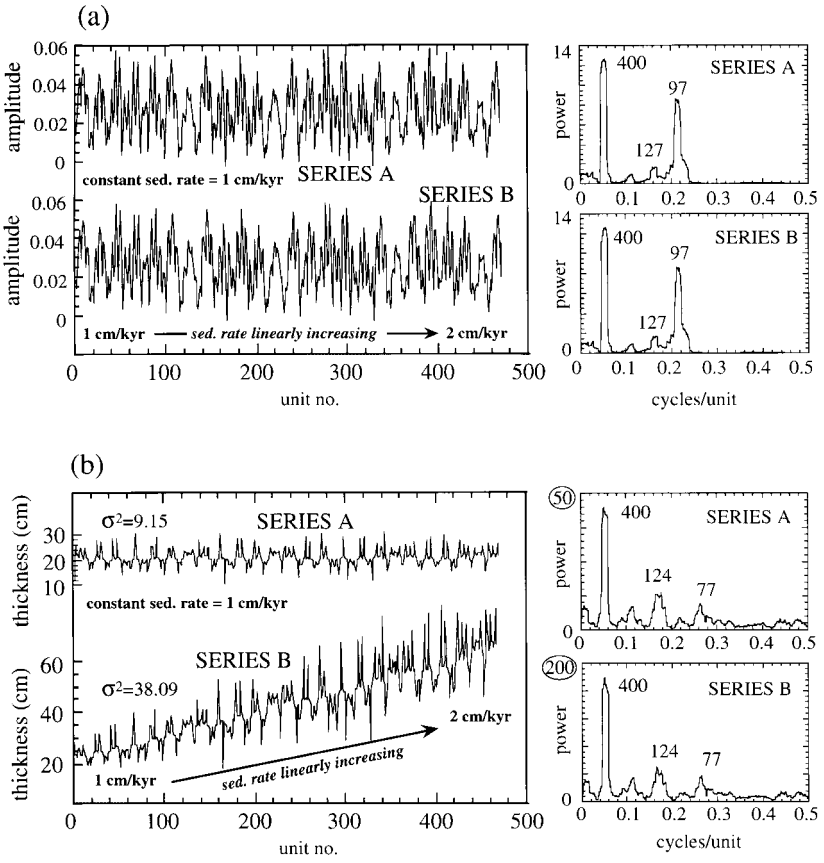

Figure 5 Metronomic measurement of the precession index-forced SERIES A and B presented in Figure 4. (*a*) *Left panel:* amplitude modulations (AM) of SERIES A and B, recorded as a function of cycle (''unit'') number; *Right panels:* 4π multi-tapered power spectra of these series. (*b*) *Left panel:* frequency modulations (FM) of SERIES A and B recorded as a function of cycle (''unit'') number; *Right panels:* 4π multi-tapered power spectra of SERIES A and B, showing containment of the increased accumulation rates in power only in the SERIES B spectrum. The change in independent variable has standardized the two series, revealing that they were forced by the same signal.

tally from orbital tuning. In fact, the metronomic approach absorbs random deviations in accumulation rate, within the cycle number increment, that orbital tuning seeks to quantify and remove through small time adjustments. In practice, these tuning adjustments never exceed the time scale of the basic target orbital cycle. Therefore, while the metronomic approach is appealing because it works only with the raw data, orbital tuning, as it is normally practiced, is nearly as benign (see example in Section 3.4).

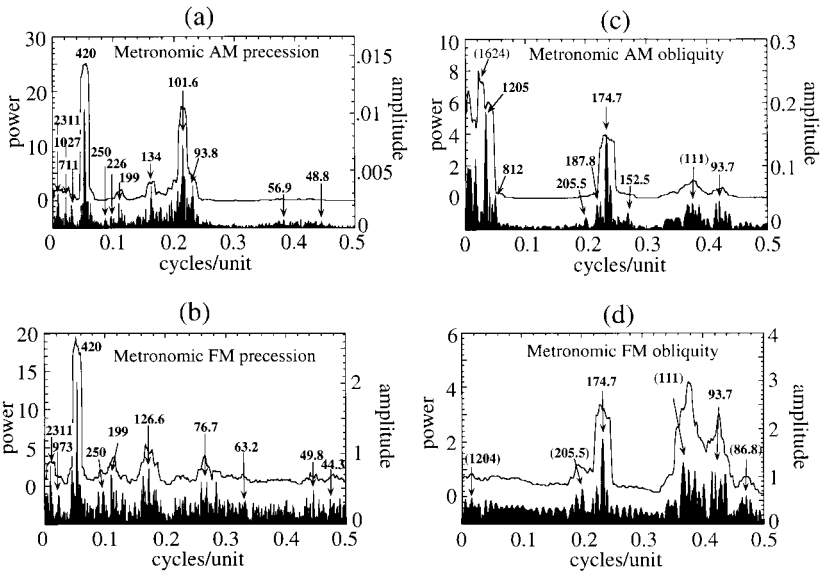

Figure 6 4π multi-tapered power spectra and harmonic analysis of metronomic AM and FM series of the precession index and obliquity series calculated over the past 10 Myrs. Power spectra are shown as *curves* (power axis on the left), and harmonic line amplitudes are shown as *black lines* (amplitude axis on the right). Labels identify harmonic lines that pass the F-test at the 99% significance level. Refer to Table 4 for summary of significant lines and their origins.

2.3.5 The Significance of Orbital Modulations The significance of AM and FM orbital patterns as they apply to stratigraphy is as follows. Changing amplitudes of precession-forced insolation cycles may be directly recorded as amplitude changes in the stratigraphic parameter under consideration, e.g. in the oxygen isotope temperature proxy. FM analysis of the proxy can be used to further assess the behavior of the underlying accumulation processes: If accumulation is stable (i.e. constant), the proxy will have AM and FM precession modes with a spectral coherency relationship that is comparable to that depicted in Figure 2*c*. If, on the other hand, accumulation rates respond linearly to precession cycle amplitude (which is high when precession cycle periods are short), then, for example, the inverse relationship between the AM and FM modes in the 100 kyr band may be diminished, or even reversed. Thus, differences in the AM/FM relationship of stratigraphic cycles from the predicted relationship of the targeted orbital signal can reveal hidden information about the stratification process (e.g. Section 3.3.2 and Section 3.4.3).

TABLE 4 Summary of metronomic frequency modulation tones of (A) the precession index and (B) the obliquity[a]

AM Modes			FM Modes		
Period (kyr)	**Origin**	**Mode (cycles/unit)**	**Period (kyr)**	**Origin**	**Mode (cycles/unit)**
A. The precession index					
2311	$g_4 - g_3$	0.0094	2311	$g_4 - g_3$	0.0094
1027	$g_1 - g_5$	0.0211	973	$g_1 - g_5$	0.0223
711	$g_2 - g_1$	0.0305	–	–	–
420	$g_2 - g_5$	0.0516	420	$g_2 - g_5$	0.0516
250	?	0.0869	250	?	0.0869
226	?	0.0962	–	–	–
199	?	0.1092	199	?	0.1092
134	$g_3 - g_2$	0.1620	–	–	–
–	–	–	126.6	$g_4 - g_2$	0.1714
101.6	$g_3 - g_5$	0.2136	–	–	–
93.8	$g_4 - g_5$	0.2312	–	–	–
–	–	–	76.7	$g_2 + g_4 - 2g_5$?	0.2829
–	–	–	63.2	?	0.3439
56.9	$g_6 - g_5$	0.3815	–	–	–
48.8	?	0.4448	49.8	?	0.4436
B. Obliquity					
1204	$s_4 - s_3$	0.0340	(1204)	$s_4 - s_3$	0.0340
812	$s_4 - s_3 + g_4 - g_3$	0.0505	–	–	–
205.5	?	0.1995	(205.5)	?	0.1995
187.8	$s_3 - g_4 + g_3 - s_6$	0.2183	–	–	–
174.7	$s_3 - s_6$	0.2347	174.7	$s_3 - s_6$	0.2347
152.5	$s_4 - s_6$	0.2688	–	–	–
(111)	$s_1 - s_4$	0.3697	(111)	$s_1 - s_4$	0.3697
93.7	$s_1 - s_3$	0.4378	93.7	$s_1 - s_3$	0.4378
–	–	–	(86.8)	?	0.4722

[a]Periods in kyr were estimated by dividing the estimated mode values into 21.7 kyr for the precession index, and into 41 kyr for the obliquity. The g_m and s_m are as in Table 1.

3. THE EVIDENCE: ORBITALLY FORCED STRATIGRAPHY

3.1 CASE 1: Time Series Analysis of Discontinuous Cyclic Strata

3.1.1 Time and Cycles A first-order estimate of the timing (or accumulation rate) of a basic sedimentary cycle in a sequence can be approached several ways: (*a*) Divide the total time represented by the cyclic sequence by the total number of cycles; or (*b*) estimate the average accumulation rate for the entire sequence by dividing its total thickness by the total time. This means that if, for example, the cycles become progressively thicker upsection, (*a*) will predict that accumulation rates for cycle deposition must be increasing, whereas (*b*) will infer that the time of formation of individual cycles is increasing. Which of the two approaches is the correct one is open to debate. One could argue that cyclic processes tend to be time-invariant, in which case (*a*) would give the right answer. On the other hand, natural processes operating within a complex system of driving forces may drift and come to interact with different forces, thus raising the possibility that the cycles can experience timing changes. This has been observed in stratigraphy, for example, when the Pleistocene glaciations changed from 41 kyr to 100 kyr timescales (see Section 3.3). One remedy is to apply metronomic AM/FM analysis to determine whether an orbital signal is associated with the cyclic sequence. If the timing (accumulation rate) of the basic sedimentary cycle can be established as the product of orbital forcing, then an incremental time scale can be developed within the cycles through application of other accumulation rate models (see example in Section 3.1.3).

3.1.2 γ-Analysis When confronted by cyclic stratigraphy composed of a repeating sequence of facies, it is reasonable to hypothesize that each facies accumulated at a unique rate within the cycle, and that each facies accumulated at the same rate in each of the cycles in the sequence. The γ-method proposed by Kominz & Bond (1990) tests this hypothesis by application of the time model:

$$T_{cy} = \sum_{n=1}^{N} \gamma_n X_{m,n} \quad m = 1, \ldots, M. \tag{8}$$

T_{cy} is the time it takes to deposit a complete stratigraphic cycle, $X_{m,n}$ is the thickness of the *n*-th facies in the *m*-th cycle, and γ_n is the (inverse) unknown accumulation of the *n*-th facies. The γ_n may be solved for M cycles $\geq N$ facies, using generalized linear inversion methods (e.g. Menke 1989, Hjelt 1992).

A number of assumptions need to be taken into account when applying γ-analysis. The principal assumptions are (*a*) the basic stratigraphic cycle is deposited over a constant period T_{cy}; (*b*) proportionate thicknesses of the facies within the stratigraphic cycles are consistent from cycle to cycle; and (*c*) facies thickness

is directly proportional to time. Regarding (*a*), stratigraphic cycles that were orbitally forced by the obliquity or precession index only will have experienced cycle period variations of $\pm 7\%$ and $\pm 15\%$, respectively, so one question is whether the γ-method is robust to such variations. To test this, Woronow (1992) applied γ-analysis to synthetic data with a coefficient of variation of $\pm 15\%$ in T_{cy}, and for $N=3$ and $M=4$ was unable to recover reasonable estimates of the true facies accumulation rates. Kominz & Bond (1992), however, argued that the method needs to be tested over $M>>N$ cycles and that the results should be examined as an ensemble by spectral analysis averaged over all of the cycles. They found that a coefficient of variation as high as 40% in T_{cy} would result in a γ-corrected time series that is still significantly improved over one based on a uniform (average) accumulation rate for all of the facies. This implies that the method can be applied successfully even to stratigraphy with mixed obliquity-precession index cycles. For (*b*) to hold, the facies must have unique accumulation rates and/or similar (environmental) conditions that consistently lead to facies preservation from cycle to cycle. This means that secular drifts in rates over the long term is not permitted. Finally, (*c*) tends to assign thicker facies more time than thinner ones. This can lead to problems if, for example, a relatively thin compacted facies represents the same amount of time as another, thicker uncompacted facies within a cycle.

3.1.3 The Jurassic Domaro Limestone A recent example illustrating the practical pros and cons of γ-analysis comes from an Upper Pliensbachian sequence of basinal limestone/shale couplets from the Domaro Limestone in the Lombardy Pre-Alps, northern Italy (Hinnov & Park 1998). Metronomic FM analysis (as discussed in Section 2.3.2) of a sequence of 160 couplets from the formation revealed that the couplet thicknesses modulated with frequencies consistent with metronomic FM precession (Hinnov & Park 1998; compare their Figures 7 and 11). This led to an attempt to extract the original precession index signal by reconstructing the incremental time scale along the sequence. The a priori information for precession index forcing supplied by the FM analysis was a sufficient criterion for application of γ-analysis and setting T_{cy} = average Early Jurassic precession cycle duration (19.4 kyr was assumed in their model). Advanced FM modeling in Hinnov & Park (1998) suggested that limestone had been deposited during one half of each precession cycle and shales during the other half, which invites the hypothesis that the limestones and shales each on average represent the same amount of time (9.7 kyr).

These models are summarized in Figure 7. The original stratigraphic series (Figure 7*a*) has a 10:1 thickness contrast between the limestones and (highly compacted) shales; its power spectrum (Figure 7*b*) exhibits a multitude of peaks with comparable power, a condition symptomatic of the discontinuous nature and extreme deviation from sinuosity of the input series. The γ-estimated time model (Figure 7*c*) stretches the shales relative to the limestones, by assigning them 1/3 of the total cycle time. Its power spectrum (Figure 7*d*) reveals that the γ-model

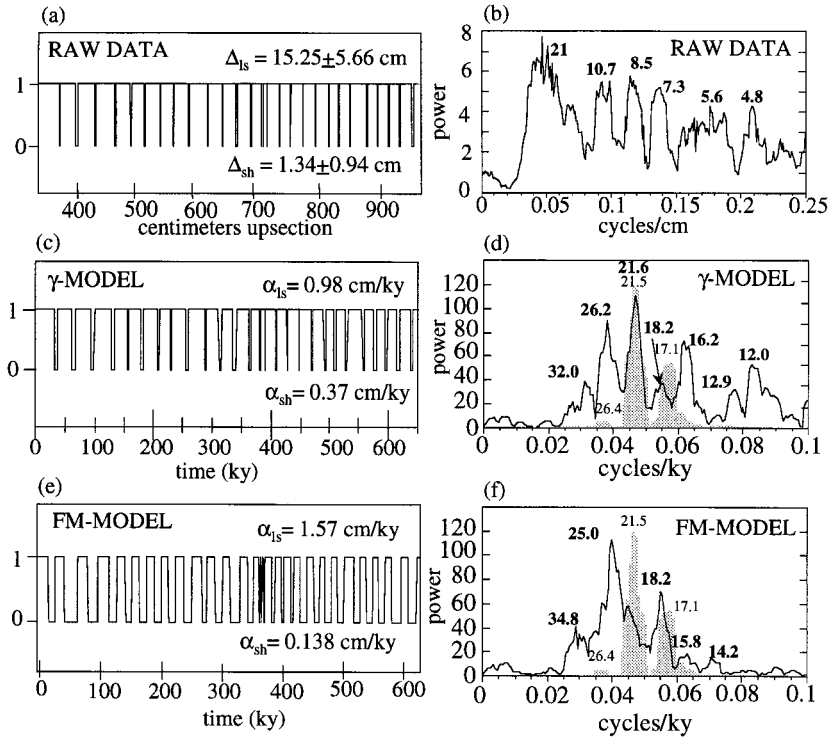

Figure 7 Analysis of the Pliensbachian Domaro Limestone limestone/shale couplet sequence, from Hinnov & Park (1998, 1999) and Hinnov et al (2000). The sequence was analyzed as a lithologic rank series, with limestones recorded with the value 1 and shales with the value 0. (*a*) The raw rank series of Couplet nos. 24–51, recorded as a function of stratigraphic position and interpolated to a 0.01 cm spacing. (*b*) 2π multi-tapered power spectrum of the interpolated data, Couplet nos. 24–74. (*c*) The couplets in (*a*) recorded as a time series at 200-year spacings, using accumulation rates estimated by the γ-method (Kominz & Bond 1990); (*d*) 2π multi-tapered power spectrum of the γ-model applied to Couplet nos. 24–74. (*e*) Couplets in (*a*) recorded as a time series at 200-year spacings, using accumulation rates according to the FM model (Hinnov & Park 1998). (*f*) 2π multi-tapered power spectrum of the FM-model applied to Couplet nos. 24–54. The shaded spectrum is that of a 1 Myr–long precession index signal with values truncated to 0 and 1 to simulate the discontinuous nature of the data. Labels in (*b*) are in cm; labels in (*d*) and (*f*) are in kyrs.

has significantly reduced spectral variability. The dominant spectral peak coincides with that of a boxcar precession index model; however, numerous other peaks are present that are not obviously related to a precession index spectrum. Finally, the FM time model (Figure 7*e*) balances the amount of time spent in the limestones and shales; time variations along the series are the result of the thick-

ness variations of the lithologies that occur from couplet to couplet. The power spectrum (Figure 7*f*) shows sharpening of the spectrum into two major peaks that is more consistent with the precession index spectrum. Evolutionary spectral analysis of this model in Hinnov et al (2000) shows that these frequencies are slightly unstable within the analyzed 1 Myr window, and shift to slightly higher frequencies in the latter half of the interval. This probably accounts for the displacement of the two peaks relative to those of the precession index spectrum.

The FM evidence for precession index forcing of the Domaro couplets formed the basis for the development of both time models. However, the γ-model's linear solution apportions thickness linearly with time, with the result that the limestones, on average 10 times thicker than the shales, are assigned the bulk of the total cycle time. In fact, pandpass tests (Hinnov & Park 1998) indicate that the covariant contrast between limestone and shale thicknesses within cycles is closer to *ca.* 3:1; this is reflected in the γ-estimated accumulation rates for the two lithologies in Figure 7*c*. The ability of γ-analysis to recover true time scales within cyclic strata may prove to be one of its weaker attributes because of unexpected facies behavior, long-term accumulation rate change, and so on, that may be difficult to anticipate. However, the method rapidly assesses linear proportionality among cyclic facies, and thus can serve as a general statistical test for nonrandomness within cyclic strata.

3.2 CASE 2: High Resolution Optical Densitometry

3.2.1 The Cretaceous Piobbico Core A remarkable example of cyclic stratigraphy that is too old to yield primary marine isotope climate proxies, and that has proved too expensive to sample in detail in its entirety, comes from the Middle Cretaceous Piobbico core. This 80 meter–long core was drilled in 1979 through the pelagic Fucoid Marls in the northern Apennines (central Italy), an Aptian-Albian succession of cm-dm scale marly carbonate/shale cycles. In outcrops close to the drill site, the formation shows striking cyclicity and continuity, with well-defined lighter (carbonate-rich) and darker (carbonate-poor) alternating sediments (De Boer 1982) indicating strong redox variations superimposed on a basic carbonate productivity cycle. The principal objective for drilling was to obtain superior vertical control of the formation and perform precision sampling and stratigraphic analysis. A summary of the core's biostratigraphy, magnetostratigraphy, and cyclostratigraphy is given in Larson et al (1993), who subsequently expanded sampling to another site at Cismon (Bellanca et al 1996).

3.2.2 The Amadeus Interval Detailed study of sedimentary cyclicity in the core was confined largely to the Upper Albian (Herbert et al 1986, Herbert & Fischer 1986, Park & Herbert 1987, Ripepe & Fischer 1991, Fischer et al 1991, Erba & Premoli Silva 1994), a *ca.* 1.6 Myr–long segment that later came to be known as the Amadeus Interval (Coccioni & Galeotti 1991). The high-frequency cyclicity was documented from Meters 9.6–16.8 (stratigraphic depth) by cm-scale sam-

pling for elemental analysis; spectral analysis of the weight percent carbonate series (Park & Herbert 1987) and aluminum series (Herbert 1994) was applied to search for orbital signals. Both in nearby outcrops and within the core, black/white color variations clearly define individual couplets that are grouped into sets of five to six, which is suggestive of precession index-forced sedimentation. Surprisingly, however, neither the sampled series nor a high-resolution densitometric scan of the clearly visible color variations recovered prima facie evidence for the precession-scale cycles (Park & Herbert 1987, their Figure 2; see also Section 3.2.4).

3.2.3 High-Resolution Optical Densitometry The precession cycle detection problem was recently revisited by Grippo et al (1998, 1999), who scanned for grey-scale variations at a 0.8 mm spacing along a single pixel transect of digitized photographic images of the original polished Amadeus core segments. The procedure is described in detail in Grippo et al (in review). Figure 8 displays the Grippo grey-scale scan along with the original weight percent carbonate series assembled by Herbert et al (1986), who also produced a high-resolution densitometric scan of the series from the same photographs (also shown). The Herbert scan, though performed at a 0.2 mm resolution, represents the average (stack) of 25 adjacent scans of the photographs. Despite its much higher resolution, the Herbert scan appears to be much smoother than the Grippo single scan. This is because the stacking effectively ''mixed'' lateral color variations within strata from incidental burrows, fractures, photo blemishes, etc. This horizontal mixing blurs and diminishes the amplitude of the cycle transitions—in particular, from the white carbonate units to succeeding thinner, well-defined black shales, which are readily picked up by the Grippo single scan.

3.2.4 The Milankovitch Band In Figure 9, the carbonate power spectrum shows clear symptoms of undersampling with reduced power levels in the precession band. The choice for a *ca.* 2-cm sampling rate had been premised on the expectation that the precession-scale couplets, the highest frequency of interest, were *ca.* 8 cm thick; 4 samples per couplet should have been adequate to recover good statistics for the basic couplets. (The sampling rate was also narrowed considerably within shalier intervals to ensure that all of the couplets were fully sampled.) However, Park & Herbert (1987) noted that the longer *ca.* 50 cm–thick cycle bundles, interpreted as an expression of 100 kyr eccentricity, show substantial changes in thickness within the Amadeus Interval. These were interpreted as the results of accumulation rate fluctuations ranging over a factor of 2 (Park & Herbert 1987, their Figure 9). This can be observed in the Grippo power spectrum, where the suite O, P1 and P2 occur also at higher frequencies with lower power (see dashed arrows, small labels).

This wide range in accumulation rates guarantees that a certain number of the high frequency cycles will be undersampled by $\Delta d = 1.9 \pm 1.1$ cm, which has a variable Nyquist frequency ranging as low as $1/(2 \cdot 4.1 \text{ cm}) = 0.122$ cycles/

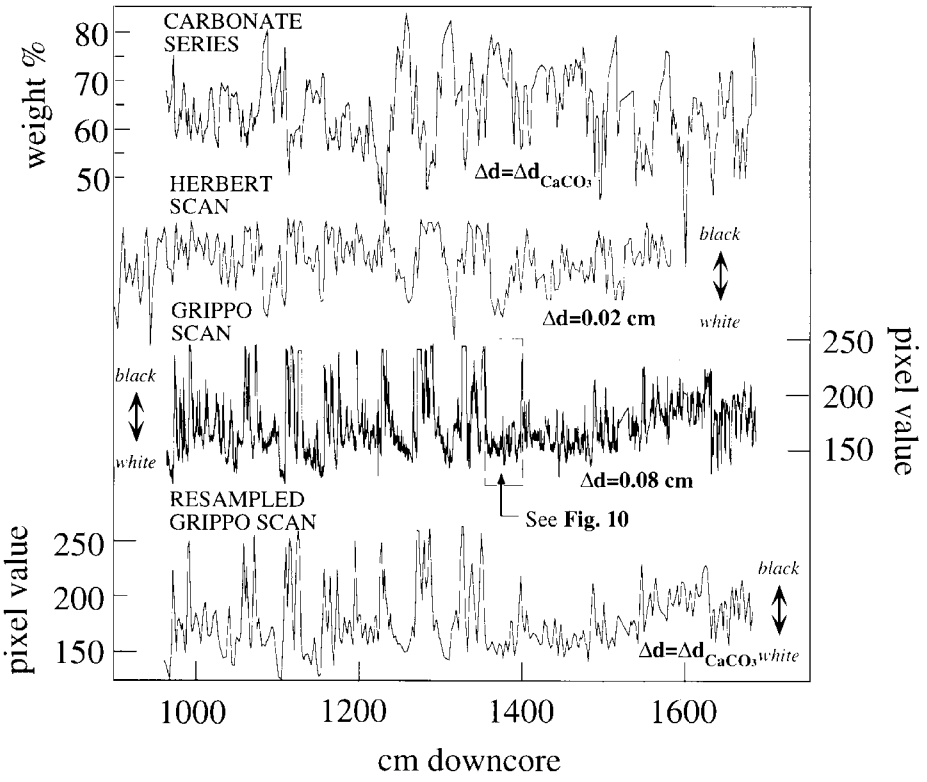

Figure 8 Paleoclimatic series collected from the Amadeus Interval of the Middle Cretaceous Fucoid Marls (*Ticinella praeticinensis* zone, Upper Albian) cored at Piobbico, northern Apennines, Italy. From *top to bottom:* CARBONATE SERIES—collected at variable $\Delta d = 1.9 \pm 1.1$ cm intervals and analyzed by Herbert et al (1986), Herbert & Fischer (1986), Park & Herbert (1987), and Herbert (1994). HERBERT STACKED SCAN—the average of 25 adjacent light transmission scans taken at 0.2-mm spacings of core segment photograph diapositives, and analyzed by the same authors. GRIPPO SINGLE SCAN—the results of a new single pixel–wide scan taken at 0.8-mm spacings of digitally imaged versions of the same core photographs (Grippo et al 1998, 1999). The box labeled A indicates the segment analyzed in Figure 10. RESAMPLED GRIPPO SCAN—the GRIPPO SINGLE SCAN resampled at Herbert's variable carbonate series sampling grid, to study the effect of the sampling on the high frequencies. From Grippo et al (in review).

cm (lower 95% confidence limit). If the Grippo scan represents more fully the ''true'' cyclic variations in the Amadeus Interval, then applying the Herbert sampling grid to the Grippo scan should provide details about the sampling effects of the grid. The resampled Grippo scan (Figures 8 and 9) was sampled only at the stratigraphic positions where Herbert collected samples. To simulate the *ca.* 1-cm diameters of the collected samples, the recorded pixel values were averaged

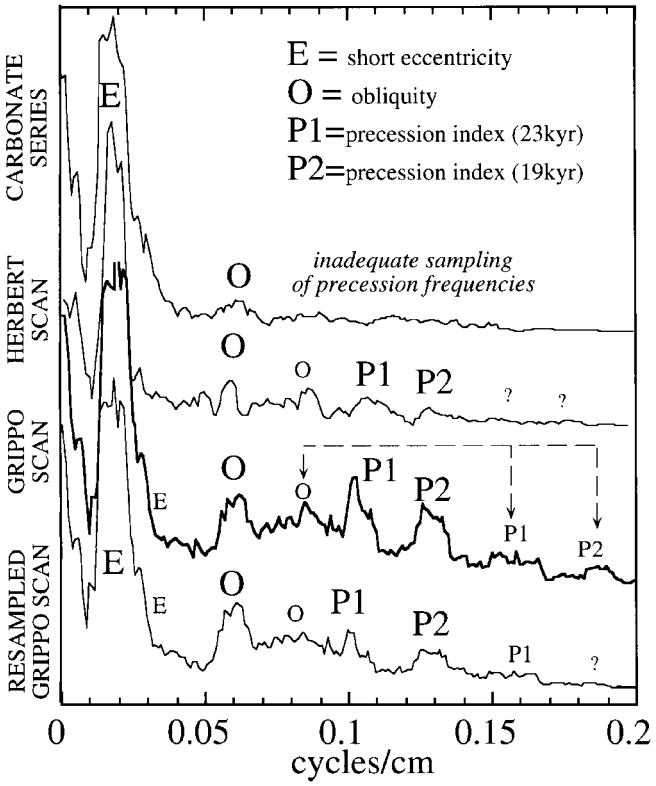

Figure 9 Multi-tapered power spectra of the paleoclimatic series in Figure 8. 4π multi-tapers were applied to all series except the HERBERT STACKED SCAN, to which 3π multi-tapers were applied. Calibrating the spectral peak labeled ''O'' at a 41 kyr period results in P1 = 23 kyrs, P2 = 19 kyrs, and E = 111 kyrs. The smaller labels indicate a drift of the main peaks to higher frequencies as a result of lowered accumulation rates over part of the Amadeus Interval (Herbert et al 1986, Park & Herbert 1987), during which time component E has anomalously low power. From Grippo et al (in review).

over 1-cm lengths centered on the sampled locations. The results show a marked diminution in the definition of the P1 and P2 peaks; this confirms that the sampling grid significantly undersampled precession components within the interval, with deterioration occurring even at peak ''o'' at 0.08 cycles/cm. A full simulation of the sampling effect would have involved calculating the average pixel value over a 0.5 cm radius around each sampled location, but this was too time-consuming to perform with the available imaging software. (In this respect, the Herbert stacked scan comes closer to reproducing Herbert's sampling grid.)

3.2.5 The Sub-Milankovitch Band The Grippo scan, with its 0.8-mm resolution, far below the 8–10 cm precession-scale cycle wavelengths, provides a unique opportunity to examine the sub-Milankovitch band. Figure 10 documents a curious multiplet variation that characterizes portions of the scan at the 1- and 2-cm scale. Figure 10*a* shows a full *ca.* 100 kyr eccentricity cycle from Meters 13.52–13.94, in which individual precession index cycles and obliquity cycles are clearly visible; superimposed on these is another order of much lower-amplitude, high-frequency variations. High-resolution harmonic analysis of the segment (Figure 10*b*) indicates that these high frequencies are dominated by two stable harmonic lines at f = 0.52 and 0.94 cycles/cm. Closer examination (Figure 10*c*) confirms the presence of pervasive 1-cm cycles grouped into 2-cm ''doublets'' throughout the segment. The doublet arises in several (relatively carbonate rich) segments in the Grippo scan, although the example in Figure 10 depicts its most striking appearance. The amplitude of the doublet variation is only about 25% of the average amplitude of the precession cycles. Its high degree of regularity is unusual for stratigraphy, and indicates the presence of millennial-scale 5.0 kyr and 2.5 kyr pulses in the stratification process (Grippo et al, in review).

Millennial-scale periodicity was first reported in the North American Permian Castile Formation, a climatically driven evaporite sequence in which anhydrite-calcite carving was interpreted to represent the annual cycle (e.g. Anderson 1982, Anderson & Dean 1995). Over measurements of 200,000 varves, anhydrite laminae thicknesses revealed a major oscillation with an average 2.7 kyr period riding on a clearly discernible lower-amplitude precession index/eccentricity background—the response of a high-frequency variation in the hydrologic cycle. The Late Pleistocene Estancia Lake in the same region shows sedimentary cycling at the same scale (Allen & Anderson 1993). The high-resolution Pleistocene deep-sea record has also revealed high-amplitude millennial-scale climatic modes (e.g. Pestiaux et al 1987, Hagelberg et al 1994, Bond et al 1997), as has the Greenland ice core GISP2 (Dansgaard et al 1993), which is in turn correlated with millennial-scale anoxia cycles in the Santa Barbara Basin sediments (e.g. Behl & Kennett 1996, Hendy & Kennett 1999, Cannariato & Kennett 1999). This scale of climatic variability seems to be age-independent: Pronounced millennial-scale basinal rhythmites have also been reported in a number of Paleozoic formations in western North America (Elrick et al 1991, Elrick & Hinnov 1996).

3.3 CASE 3: The Hundred Thousand Year Problem

3.3.1 The Late Pleistocene Ice Age The Late Pleistocene 100 kyr glaciation cycles are undoubtedly the most scrutinized phenomenon in paleoclimatology. Literally dozens of models have been proposed to explain these cycles; a short list is given in Imbrie et al (1993, their Table 3). Many of these models embrace the idea that the 100 kyr timing of the cycles is fundamentally a response that can be traced to Earth's orbital eccentricity. The remarkable amplification of the glaciations of the minute insolation forcing power provided by the eccentricity

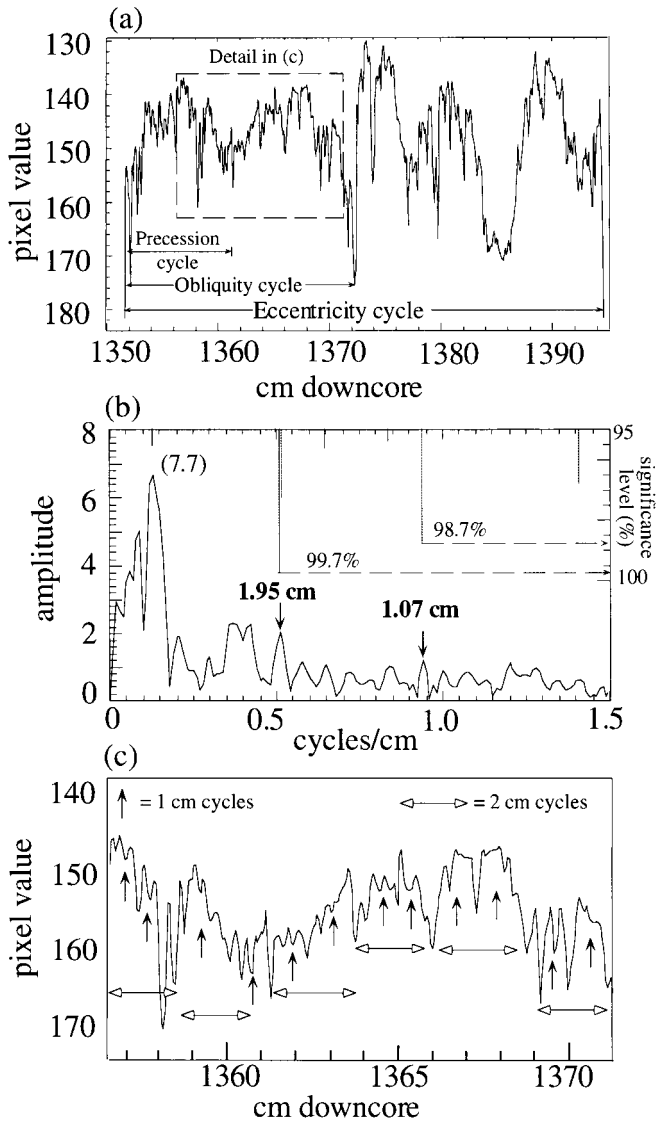

Figure 10 High frequencies recorded in the Grippo Single Scan. (*a*) A segment from Meters 13.52–13.94 (see Figure 8 for position within the scan), interpreted as a full eccentricity cycle, with five precession index oscillations and two obliquity cycles clearly visible. (*b*) 2π multi-tapered harmonic analysis of the interval, with results of F-tests for harmonic lines shown at the top. The precession cycles occur within this segment at an average 7.7-cm wavelength just exceeding 95% significance level; two highly significant lines occur at average wavelengths of 1.95 cm and 1.07 cm at less than a third of the amplitude of the precession. (*c*) Detail of the segment reveals that the source of the harmonic lines in (*b*) is 1-cm cycles grouped into 2-cm cycles (see arrows). From Grippo et al (in review).

has been explained variously as the combined response to a variety of positive feedbacks, to development of free *ca.* 100 kyr oscillations in large ice sheets unrelated to eccentricity, and to other (non)linear interactions involving the atmosphere, oceans, cryosphere, and solid Earth. Among these, simple models that couple the large scale dynamics of ice sheets, tectonics, atmospheric CO_2, and ocean thermal state produce internal 100 kyr scale oscillations (Saltzman & Sutera 1987) that come to be entrained by external orbital forcing (Saltzman & Maasch 1990). More recently, 100 kyr climatic responses were obtained by direct orbital forcing of a 2.5-dimensional model of the Northern Hemisphere linking atmospheric circulation and CO_2, sea ice, land-based ice sheets, and other continental surface conditions (e.g. Berger et al 1999).

3.3.2 Other Recent Work A number of other studies have approached the Pleistocene problem through examination of intrinsic time-periodic properties of the orbital parameters (Figure 11). Although eccentricity has long been targeted as a likely cause of the 100 kyr cycles, the difficulties in assigning physical mechanisms to generate the necessary gain to power the cycles led Liu (1992) to examine frequency resonance phenomena among the orbital parameters as an alternative source for the variation. Liu observed that the Earth's obliquity cycle modulates in frequency with a major 100 kyr periodicity that is intermittently phase-locked with *de/dt.* Liu showed that this locking is the result of libration between Earth's obliquity and variable solar torquing produced by changes in orbital eccentricity. Liu (1995) speculated that the 100 kyr glaciations were therefore the product of nonstationary synchronization between the obliquity and eccentricity, with sustained synchrony triggering 100 kyr-scale pulsations in Earth's climatic response during the Late Pleistocene. Independently, Rial (1995) noted that the δ18O signal evolves as the first derivative of the orbital eccentricity, *de/dt.* This explained both the sawtooth pattern of the glaciation signal and the absence of the 400 kyr eccentricity cycle. Rial's interpretation was that rapid switches from cooling to warming occur as orbital eccentricity passes through minima (near-circular orbits), when warming rates kick in at maximum value. The likely power source of the forcing would be the high-frequency precession index, which carries the eccentricity variation. Subsequently, Liu (1998) explored the effect of a bipolar pulse-modulated insolation forcing on a zero-dimensional energy balance model and was able to reproduce all major trends in the Pleistocene $\delta^{18}O$ record in an output temperature time series (Figure 11, bottom two series). The pulse modulation model infers a two-sided threshold response of the global climate to conditions involving a cooperation between instantaneous insolation amplitude and frequency. Prior to 1.2 Myrs b.p., the dominant orbital component in both the model and data is the 41 kyr obliquity cycle. From 1.2–0.9 Myrs b.p., a component with an ~80 kyr periodicity briefly dominates the model signal; this subsequently evolves into a 100 kyr signal that dominates the signal from 0.9 Myrs b.p. to the present, the result of intensification of time-pulsation effects from a continuously improving synchronization between *de/dt* and FM

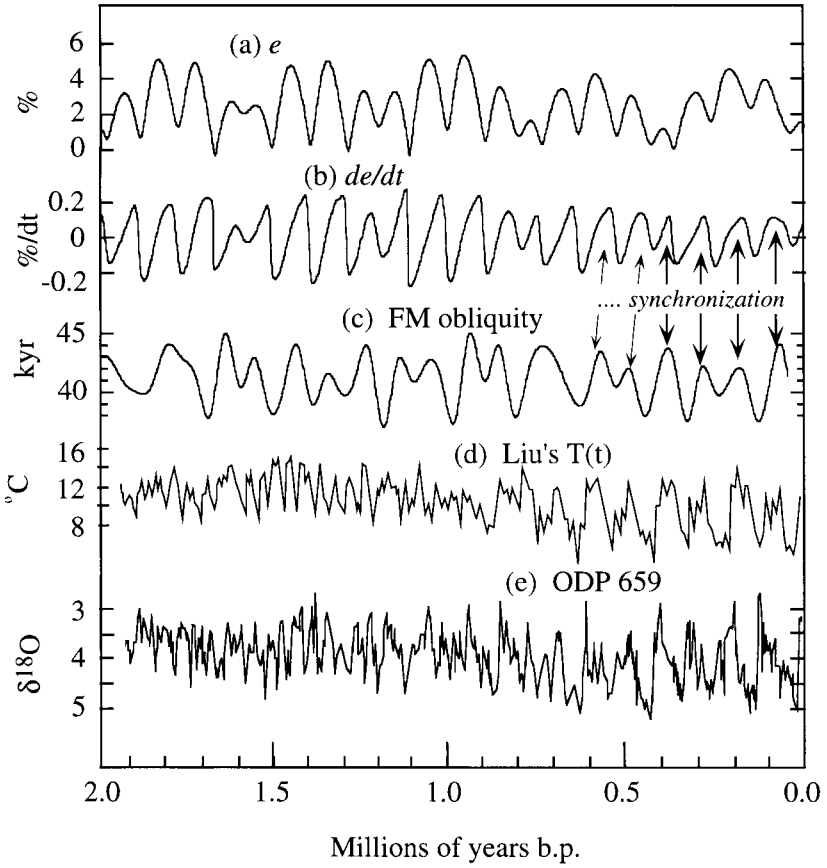

Figure 11 Summary of 100 kyr orbital phenomena thought to be related to the forcing of the Late Pleistocene glaciation cycles, for 0 to 2 Myrs b.p. (*a*) Eccentricity *e* from the La90(0,1) orbital model. (*b*) First time derivative of the eccentricity, *de/dt*, showing a sawtooth pattern and suppression of the 400 kyr component (after Rial 1995). (*c*) Frequency modulation of the obliquity. (*d*) Zero-dimensional energy balance model of Liu (1998). (*e*) Oxygen isotope record of ODP 659 from Tiedemann et al (1994).

obliquity. In addition, the modeled 100 kyr cycles slowly modulate with a 400 kyr periodicity (Liu 1998, his Plate 1), as do the 100 kyr cycles in the $\delta^{18}O$ record over the same time interval (Rial 1999, his Figure 1).

Liu's model shows that a 100 kyr resonance phenomenon has developed between Earth's obliquity and eccentricity over the past million years. The apparent phase lock of this resonance with the marine isotope record (as illustrated in Figure 11) may point to the origin of the long-noted misfit between the data and orbital eccentricity. It may also be that other orbitally forced Pleistocene models capture elements of this resonance in their 100 kyr outputs. Of additional note is

that successful replications of the stepwise evolution of the Pleistocene 100 kyr glaciations by these models are possible only with the aid of a second external agent—i.e. a secularly decreasing atmospheric CO_2. In this respect, Liu's scheme offers an important alternative solution to the 100 kyr problem should it come to pass that the CO_2 proxy data—yet to be collected—do not corroborate the postulated Late Cenozoic CO_2 decline (see Pagani et al 1999 for data controverting a postulated decline during Miocene times).

3.3.3 Orbital Inclination Muller & McDonald (1995, 1997a,b) proposed yet another hypothesis: Earth's variable orbital inclination *I*—not eccentricity—caused the 100 kyr glaciations. These researchers argued that the $\delta^{18}O$ record showed no evidence for the triple 404 kyr, 127 kyr, and 95 kyr components that characterize eccentricity, but exhibits a single, narrow-band 100 kyr spectral peak. This spectral structure is more consistent with *I*, which has a dominant 98 kyr cycle (Quinn et al 1991). Muller & McDonald hypothesized that during times of low *I*, the Earth's orbit intersects an interplanetary cloud of dust and meteoroids; the proposed climatic effects of extraterrestrial dust on the atmosphere remains highly speculative, however. Objections arose against Muller & McDonald's conclusions about the $\delta^{18}O$ spectrum: Rial (1999) showed that the 100 kyr component of the $\delta^{18}O$ record is frequency-modulated by a 400 kyr cycle, which is consistent with a nonlinear response of climate to eccentricity. Ridgwell et al (1999) likewise supported a Milankovitch origin, pointing to recent climate models that transform orbitally forced insolation into a predominantly single component 100 kyr glaciation response. They speculated that a superposition of obliquity and eccentricity effects was involved. This, of course, was independently proposed and modeled by Liu. In addition, Liu (1999) has shown that the frequency modulation of the obliquity, which he favors as a major player in the 100 kyr glaciations, is caused by *I*.

3.4 CASE 4: Solar System Resonance in Stratigraphy

3.4.1 Earth-Mars Resonance The fundamental frequencies g_m define the secular rates of revolution of the orbital perihelia of the planets, i.e. the major axes of their eccentric orbits, relative to a fixed sidereal reference frame. Quasiperiodic alignments between orbital perihelia are indicated by ''beat'' frequencies among the g_m; these directly affect Earth's orbital eccentricity (Table 2A, column 6). The fundamental frequencies s_m indicate the rates of revolution of the ascending nodes (i.e. the lines of intersection) of orbital planes relative to a fixed ecliptic. This motion is caused by changes in the orbits' inclinations relative to this fixed ecliptic. Quasiperiodic alignments between ascending nodes induce the modulations in Earth's obliquity (Table 4B).

Laskar (1990, 1992) showed that long-term resonance exists between the motions of Earth and Mars such that $(s_4 - s_3) - 2(g_4 - g_3) = 0$. A second libra-

tional mode also exists at $(s_4 - s_3)$–$(g_4 - g_3) = 0$. Transitions between these two modes are associated with chaotic motions of the planets. The mode g_4–g_3 is present in Earth's orbital eccentricity as a *ca.* 2.45 Myr period component (Table 2A), and should appear in stratigraphy as a modulation component in precession index-forced stratigraphy; $s_4 - s_3$, which has a period of *ca.* 1.25 Myrs, should be detectable in the modulation envelope of obliquity forced stratigraphy. Laskar (1999) urged the stratigraphic community to look for these resonance modes in the geologic past—in particular, for the most recent transition from 1:1 to 1:2 resonance. Information on when this occurred would provide important constraints on the orbital solution parameters that could significantly improve the model's validity. Laskar's calculations suggest that this transition occurred sometime before 20 Myrs b.p. (Laskar 1990, his Figure 2), so an obvious place to start the search is in the Miocene-Oligocene.

3.4.2 The Oligocene-Miocene The recent recovery of millions of years of Oligocene-Miocene orbital-scale chalk cycles from the Ceara Rise in the western equatorial Atlantic provides a unique opportunity to seek evidence for the $g_4 - g_3$ and $s_4 - s_3$ modes in obliquity and precession index-forced stratigraphy. Shackleton et al (1999b) performed complex demodulation on a 10 Myr-long, spliced, orbitally tuned record of magnetic susceptibility to examine the amplitude modulations of 21 kyr and 41 kyr components in the record. Magnetic susceptibility correlates inversely with weight percent carbonate (e.g. Weedon et al 1997). The results in Figures 6 and 7 of Shackleton et al (1999b) reveal that these AM series contain the major AM components of both the precession index and the obliquity (compare their Figure 7 with Figures 2 and 3 in this article). Although the AM series of the 21 kyr component does not reveal a 2.45 Myr periodicity indicative of $g_4 - g_3$, the 41 kyr AM series contains a strong 1.25 Myr component—i.e. evidence of $s_4 - s_3$.

Shackleton et al used a multiple-step orbital tuning strategy to obtain their spliced time series. First, they matched the amplitude modulations of the dominant lithologic cycles in the series with those of obliquity calculated above and below 23.8 Myrs b.p., the currently accepted date for the Oligocene/Miocene boundary (last appearance of *S. delphix*). A substantial downward shift of this date along the core was required to align the modulations, which resulted in an adjustment of Oligocene/Miocene boundary to a date some 0.9 Myrs younger than the currently accepted date of Berggren et al (1995). They then tuned this shifted data to an obliquity-dominated orbital target curve ''equivalent to the pattern of varying insolation at 65°N integrated over seven months centered on midsummer'' (Shackleton et al 1999b, p. 1918).

3.4.3 Metronomic Modes Metronomic AM/FM analysis can help settle the issue of whether or not the orbital tuning procedures could have biased these results. The ODP Site 926B core data used in Shackleton et al's spliced record provides the most complete raw depth series for analysis (Figure 12*a*). Eight interruptions

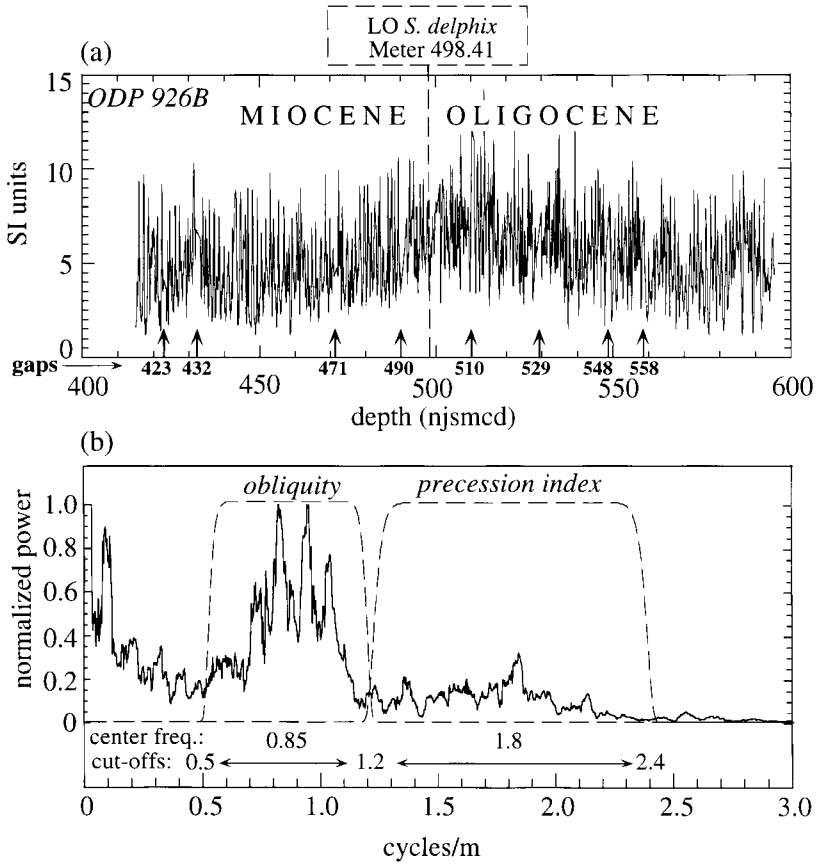

Figure 12 (*a*) Magnetic susceptibility series of the ODP Site 926B core across the Oligocene/Miocene boundary (from Shackleton et al 1999b). Depth scale is in meters. Eight gaps are shown, none of which are larger than 1–2 obliquity cycles; a few other minor breaks also occur (not shown). The Oligocene/Miocene boundary is drawn at the last occurrence (LO) of the nannofossil *Sphenolithus delphix*. (*b*) The 4π power spectrum of the series in (*a*), showing many peaks outlining two broad bands. Accumulation rates for the core are *ca.* 2–4 cm/kyr, placing the obliquity and precession index bands as shown. The center and cutoff frequencies of the bandpass filters are noted; the roll-off parameters are 10^4 dB/octave for the obliquity filter and 10^3 dB/octave for the precession filter; both filters have near-perfect zero-phase responses at all frequencies within the cutoff frequencies, ensuring that passed cycles will suffer no time shift biases.

occur within the series; these are irregularly spaced, and the longest is only 2 meters long (*ca.* 2 obliquity cycles). The spectrum of this series (Figure 12*b*) exhibits two broad power bands calibrating roughly to the obliquity and precession index. The numerous peaks within these bands indicate the presence of unstable accumulation, with rates varying up to 40%. To obtain AM and FM series of

the obliquity and precession, the bandpass filters indicated in Figure 12*b* were applied to the raw depth series separately; AM and FM metronomic series were estimated from these filtered series, and are displayed in Figures 13 and 14.

The AM obliquity data series (Figure 13*a*) has a strong component at 1.2 Myrs that is coherent and in phase with the AM series of the obliquity. Its spectrum also shares a prominent 174 kyr component with the model, although statistical coherence between data and model is low. The inference is that at the 1.2 Myr scale, lithologic cycle amplitudes on average follow those of the obliquity (high obliquity = high magnetic susceptibility value = low carbonate). In light of the prominent 174 kyr components in both data and model, the concave shape of the

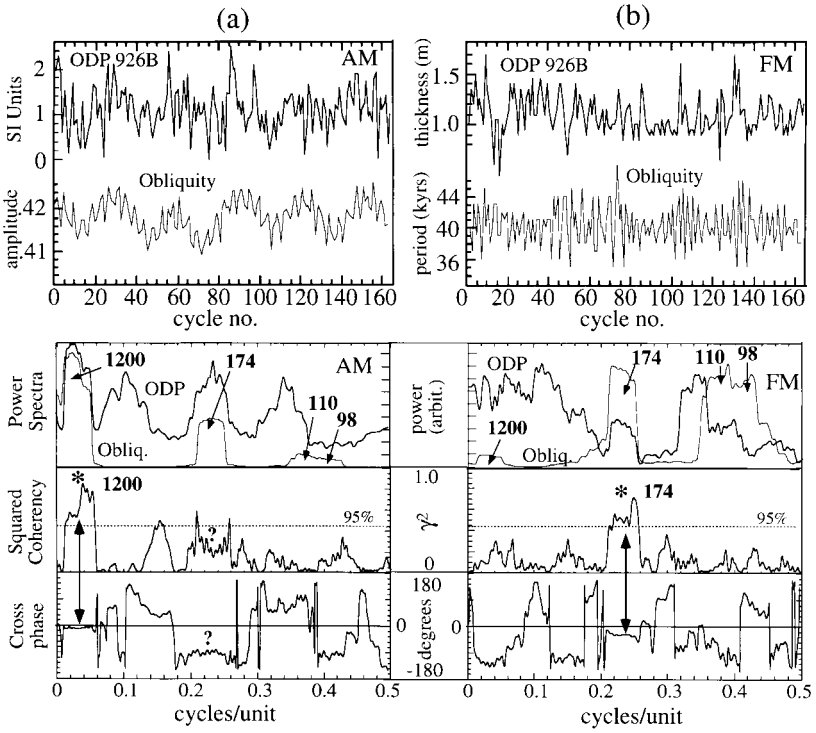

Figure 13 Metronomic AM and FM analysis of the obliquity-filtered magnetic susceptibility series of the ODP Site 926B core from Meters 415.05–595.0, compared with AM and FM series of the obliquity calculated from 20.14 Myrs b.p. (the time assigned to Meter 415.05 by Shackleton et al 1999b) to 26.7 Myrs. b.p., over a total of 164 obliquity cycles. (*a*) *Top panel:* AM series of the data and model. *Bottom panel:* 4π multi-tapered spectra of the data and model, and squared coherency and cross phase of data vs. model (negative phase indicates that data leads model). (*b*) Same as (*a*), but for the FM series of the data and model.

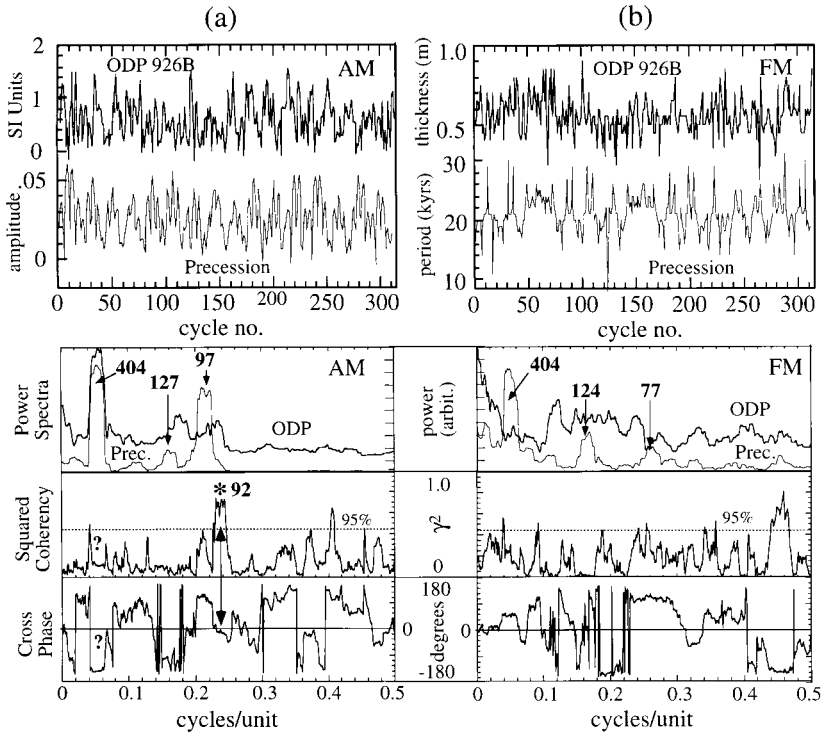

Figure 14 Metronomic AM and FM analysis of the precession-filtered magnetic susceptibility series of the ODP Site 926B core from Meters 415.05–595.0, compared with AM and FM series of the precession index calculated from 20.14–26.7 Myrs. b.p. (as in Figure 13), or a total of 322 precession cycles. (*a*) and (*b*) are as in Figure 13.

coherence curve within the 174 kyr band, along with the corresponding phase (–180° to –90°), suggest that the components are shifting continuously relative to each other throughout the series—an effect that would be expected from the progressive addition of gaps from top to bottom (see Figure 12*a*). At the same time, coherency is high between the FM components of data and model at the 174 kyr period, which indicates that cycle durations remain closely coordinated throughout the series, with a slight lead of the data over the model back through time (Figure 13*b*). Finally, the 100 kyr AM and FM obliquity modes lack coherence between data and model, although the FM data series has significant power in the 100 kyr band coinciding roughly with that of the model.

The AM precession index data series (Figure 14*a*) has a well-defined 400 kyr spectral peak that is aligned with the AM precession model; however, the pair registers low coherence. Further examination (not shown) reveals that this is because the data's 400 kyr component is progressively delayed as it encounters

additional gaps; at the base of the series, it is more than 180° out of phase with the model's 400 kyr component. This indicates a total missing time of over 200 kyrs (the eight gaps in Figure 12*a*, each about 1 obliquity cycle long, imply that 328 kyrs are missing). Two peaks are present in the AM data spectrum in the 100 kyr band, although they are shifted to slightly higher frequencies compared with AM precession spectrum—another manifestation of ''missed beats'' from gaps. At least eight 100 kyr cycles will be affected by gaps, each on the order of 40 kyrs long, or a 40% shortening of over 10% of the 100 kyr cycles in the series. High coherence occurs at a 92 kyr period between data and model, which is slightly shorter than their individual spectra, and the cross-phase is slightly unstable, once again a symptom of progressive drifting. The FM precession series for the data and model (Figure 14*b*) shows that the data has little evidence for FM precession forcing. FM orbital variations in stratigraphic cycles indicate a linear response of accumulation rates to orbital forcing. AM components can still be preserved in the event that the FM components become distorted from unstable accumulation not coupled with orbital forcing. The absence of FM precession components at ODP Site 926B indicates that accumulation rates were not coupled to precession index forcing.

In sum, metronomic analysis of the Ceara chalk recovers the same information presented by Shackleton et al, but without fine-scale orbital tuning. As is clear from Figure 12*b*, specific orbital components cannot be inferred from the raw data series, but they can be inferred from their AM and FM metronomic spectra (Figures 13 and 14). Skeptics of orbital tuning can look to this alternative technique for analysis of data; the technique also can justify the application of orbital tuning by providing a priori evidence for orbital signal in stratigraphy. It should be emphasized that the careful, cycle-by-cycle correlations performed by Shackleton et al among the various Leg 154 cores to assemble a continuous, spliced series help to infer from the outset the durations of the gaps at ODP Site 926B. Tuning to their specific orbital target curve preserves the AM and FM relationships discussed previously, although the precession index variations may have been shifted relative to those of the obliquity as a result of choice of latitude and season (Section 2.2.1) in their target curve.

The evidence for Earth-Mars resonance is restricted to observation of an s_4-s_3 mode from the 1.2 Myr component in the AM obliquity data spectrum (Figure 13*a*). The $g_4 - g_3$ mode, which should occur in the AM and FM precession spectra with a ~2.4 Myr period (*cf* Figure 2*b*), is not visible (see Figures 14*a* and *b*). The predicted strength of this modulation is very low, however. Alternatively, detection of the two AM precession components at 130 kyr and 124 kyr (Table 2A, n = 3 and 5), theoretically possible over a 6.56 Myr-long series, may supply the necessary evidence, although the repeated gaps along the series may obscure resolution of these two components. The only other strategy would be to select the longest interval between gaps, tune this to a target obliquity-only curve, and seek evidence for separate 18.9 kyr and 19.0 kyr components in the precession index band (Table 2C, n = 3 and 4).

3.5 CASE 5: Earth's Paleoprecession

3.5.1 Tidal Dissipation Earth's rotation rate has been decelerating through time as a consequence of drag caused by the offset between Earth's tide raised by the lunar potential and the Moon's lagged position relative to this tide. This perpetual offset is caused by the fact that Earth spins faster than the Moon orbits Earth. The drag is also causing a slow recession of the Moon from Earth. Both Earth's deceleration and the lunar recession have been observed directly (e.g. Morrison & Stephenson 1991, Dickey et al 1994), although their geological evolution remains largely hypothetical (Touma & Wisdom 1994). However, there have been observations for length-of-month, taken from sedimentary tidalites and coral and shell growth rings, that appear to confirm the general concept of faster spin rates and a closer Moon in remote times (e.g. Lambeck 1980).

A principal effect of tidal dissipation on Earth's orbital parameters is the shortening of k, as postulated in Table 3. With stable mode g_5 and moderately stable g_2 (Laskar 1990), changes in k may be observable in the frequency and/or amplitude modulations of ancient precession index-forced stratigraphy involving the modes $g_2 - g_5$, $g_4 - g_5$ and $g_3 - g_5$, and to a lesser extent, $g_4 - g_2$ and $g_3 - g_2$. Table 5 shows that if the evolution of k follows the model in Table 3, the modulations of the precession index will occur at lower metronomic frequencies in the remote geological past.

3.5.2 Orbital Evidence Stratigraphy appears to confirm increased k for remote times. Figure 15 shows cycle modulation spectra of three multimillion year long, precession index-forced stratigraphic sequences, from the Oligocene-Miocene (~23 Myrs b.p.), Late Triassic (~210 Myrs b.p.), and Cambrian-Ordovician (~500 Myrs. b.p.). Table 5 provides predictions for the expected frequency shifts in the major AM precession components for these geological epochs. As discussed in Section 3.4.3, the AM precession spectrum of ODP 926B suffers from effects

TABLE 5 Predicted values of modulation frequencies of the precession index at the Oligocene/Miocene, Triassic/Jurassic, and Cambrian/Ordovician boundary times[a]

Myrs b.p.	k ($''$/yr)	ω (kyr)	$\omega \cdot(g_2 - g_5)$	$\omega \cdot(g_4 - g_5)$	$\omega \cdot(g_3 - g_5)$	$\omega \cdot(g_4 - g_2)$	$\omega \cdot(g_3 - g_2)$
0	50.431631	21.7	0.053	0.229	0.220	0.175	0.167
23	50.868824	21.5	0.053	0.226	0.218	0.174	0.165
210	54.776791	19.8	0.049	0.209	0.201	0.160	0.152
500	62.173118	18.0	0.044	0.189	0.183	0.145	0.138

[a]Values of k are from Table 3 (interpolated at 23 Myrs and 210 Myrs). ω was estimated by calculating using the FORTRAN program of Berger (1978a) with updated tables from Berger & Loutre (1988), and substituting input k with the values in Column 2. The total number of cycle completions of ω over a 500 kyr test run was taken to represent its average periodicity, which is recorded in Column 3. In Columns 4–8, the modes $g_2 - g_5$, $g_4 - g_5$, $g_3 - g_5$, $g_4 - g_2$, and $g_3 - g_2$ are in kyr^{-1}, calculated from Column 6 in Table 2A.

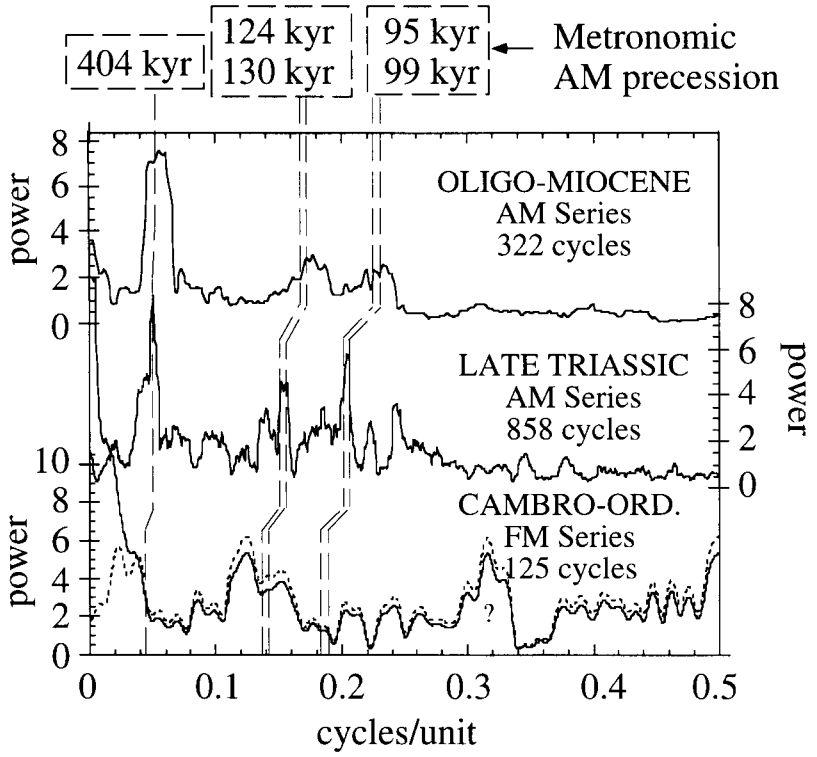

Figure 15 Metronomic cycle modulation analysis of three cyclic sequences representing the Cenozoic, Mesozoic and Paleozoic eras. The Oligocene/Miocene AM series is from the Ceara chalks (see Figure 14*a*); the Late Triassic AM series was computed from the composite rank depth series of the Newark Basin series (e.g. Olsen 1997, Olsen & Kent 1999); and the Cambro-Ordovician FM series comes from a little-known and poorly dated peritidal cyclic carbonate sequence from the Malyi-Karatau region in Kazakstan (Bazykin 1997, Bazykin & Hinnov 2000).

of small gaps interspersed throughout the series; this causes a mild ''missed beats'' problem and a shift of the AM components to frequencies slightly higher than predicted. The Late Triassic Newark AM spectrum computed from the composite rank depth series has three high-power, narrow peaks that align perfectly with all three AM precession components predicted from Late Triassic k = 54.776791″/yr, but there are other, lower-power components that require further study. The Cambro-Ordovician Ooshbas peritidal cycle thickness series is only 125 cycles long, but shows evidence for bundling: Its FM spectrum shows two peaks close to the predicted 400 kyr and 124/130 kyr components. Because it is an FM series, no peak would be expected at 95/99 kyr (the ''100 kyr hole;'' see Figure 2). Only a few other reports of apparent orbital shifts are consistent with ancient faster *k;*

this includes the Middle Cretaceous Piobbico core, in which the obliquity component occurs at a slightly shortened period of 38 kyr (Park & Herbert 1987), and the Cambrian Trippe platform carbonate cycles, which contain obliquity and precession band frequencies systematically shifted to the right from interpreted eccentricity components (Bond et al 1991).

4. CONCLUDING REMARKS

This review has surveyed some of the promising new avenues of research that have recently developed in the study of Earth's orbitally forced stratigraphy. Discussion centered on cycle pattern recognition as a principal means for identifying orbital signals in stratigraphy. Obviously, this only scratches the surface of the much larger task of linking Earth's orbital parameters to stratigraphic responses. Inevitably, to describe and explain a signal as fully as possible, the processes that led to its appearance must be identified and studied. Therefore, greater challenges still lie ahead, such as the intensive analysis of the cascade of environmental processes and their responses to orbital forcing. This applies to all of the examples discussed here, including Late Pleistocene stratigraphy, which has already been measured, parameterized, and modeled more exhaustively than that of any other epoch. Focus on potential ''sub-Milankovitch'' carriers may bring fresh insights into the field (e.g. Clement et al 1999).

Each set of data presents unique problems that require a creative and flexible approach. As demonstrated here just in grappling with signal search and recovery, no single technique is capable of leading directly to a full answer. A study design that appears to work in one case may fail when applied to another. In Section 3.1, the Jurassic Domaro limestone and shale lithologies caused havoc with conventional spectral analysis; when they were viewed as a metronomic FM series, however, an orbital signal sprang into focus. The same was true with the Cenozoic Ceara chalks (Section 3.4). Thus, an arsenal of analytical and modeling techniques is required in this discipline, and researchers should not hesitate to apply any number of them to their stratigraphic data. Finally, there are many cyclic stratigraphic sequences that will never yield their orbital signals, and there may even be a class of (auto)cyclic sequences with orbital-like spectral features that were not orbitally forced. The state of the science is not yet at the point where such non-orbital categories can be readily identified, although they have been postulated in some detail (e.g. Wilkinson et al 1998) and need to be considered as an integral part of the modeling and analysis process.

The stratigraphies protrayed in Section 3 represent a variety of climatically sensitive depositional environments: pelagic (the Cretaceous Fucoid Marls, and Plio-Pleistocene marine isotopes), hemipelagic (the Jurassic Domaro Limestone and the Oligocene-Miocene Ceara chalks), shallow marine (the Cambro-Ordovician Aisha-Bibi seamount), and lacustrine (the Newark Series). In general, strong signals would be expected to occur preferentially in long-lived lacustrine

environments, because of the extreme climatic contrasts that tend to characterize continents. However, the deep-sea records show that marine environments have also been very responsive to orbital forcing, particularly those rich in organisms producing carbonate in the tropical and paratropical zones. By far the weakest evidence for orbital forcing comes from the shallow marine carbonate record. The Cambro-Ordovician Aishu-Bibi section (see Section 3.5) typifies all of the usual problems associated with these facies. Beautifully preserved shallowing upward peritidal cycles provide a sensitive record of relative sea level change; one would expect that orbitally forced sea level oscillations would have left a strong imprint on their accumulation. However, competing forces from changes in subsidence, long-term eustasy, tidal flat progradation (autocyclicity), and prolonged intervals of non-deposition can overwhelm any nominal high-frequency component in sea level change. This can result in ''missed beats'' in the final stratigraphy, as well as irretrievable loss of signal (e.g. Goldhammer et al 1990). The Aishu-Bibi seamount was apparently no exception, and appears to have been subjected to an uneven, long-term sea level rise throughout much of its buildup (Bazykin 1997), which may have contributed to its somewhat weak record of cycle modulation.

If the ultimate objective of the stratigraphic community is to calibrate high-frequency cyclic stratigraphy with Earth's orbital parameters throughout the geologic record, then the special problems of the shallow marine carbonate record need to be studied in detail. More than half of the Phanerozoic Eon lacks a substantial pelagic marine carbonate record; carbonate-rich nannoplanktonic and microplankonic life forms did not evolve into significant (rock-forming) numbers until post-Middle Jurassic times. Therefore, the stratigraphy of carbonate platforms and of hemipelagic products shed from them into the basins are a principal resource for seeking orbitally forced signals in the Paleozoic and Early Mesozoic eras. Cyclic platform stratigraphy can be understood only through detailed modeling of the response of sedimentation dynamics of the shallow marine environment to external forcing. Modeling initiatives should be no less intensive than those that have been carried out by the glaciology and paleoclimatology communities in an attempt to explain the Late Pleistocene marine isotope signal. Today, only a handful of models are designed to study the high-frequency dynamics of carbonate platform buildups (see list in Demicco 1998). None of these models has been subjected to external forcing conditions that could be imposed from the broadband orbitally forced insolation described in Section 2, so the high frequency responses of carbonate platforms to orbital forcing remains unknown.

Finally, the focus of this review was on the Earth's precession index and obliquity, the principal parameters that control the interannual insolation. The precession index, or ''precession-eccentricity syndrome'' (Fischer et al 1991), is modulated by the eccentricity, which, as the result of climatic and stratigraphic filtering, frequently comes to be the dominant mode recorded in precession-forced stratigraphy. As demonstrated for the Oligocene-Miocene chalks (Section 3.4), analogous long-period modulations from the obliquity can also be expressed in cyclic sequences (see Hinnov & Park 1999 for a Jurassic example). It makes

sense, then, that the exploration of very long cyclic sequences—10 Myrs or longer—should consider examination of the long-period modulations of the eccentricity and FM obliquity. This may be useful, for example, in the assessment of cores that have been wirelogged over great depths at a resolution too coarse to resolve basic orbital modes, but that are clearly recording quasi-periodic modulations at the 10^6–10^7 year time scales. At the same time, however, these very low-frequency modes overlap tectonic time scales, and great care must be taken in separating these effects from the ''orbital continuum.''

ACKNOWLEDGMENTS

I would like to thank my family for the patient and perennial, moral and financial support they have given me over the past 10 years so I could pursue my interests in orbitally forced stratigraphy. I am also very grateful to Lawrie Hardie and Steve Stanley at Johns Hopkins University for their constant encouragement over the years. For this paper, Marie-France Loutre, Jacques Laskar, David Rubincam, and Jeff Park patiently fielded my questions about orbital theory, insolation, and modeling. Steve Meyers caught several important glitches in his reading of the manuscript. Han-Shou Liu kindly provided his model of Pleistocene climate. Alessandro Grippo and Alfred Fischer graciously allowed me to discuss their work-in-progress on the spectacular Cretaceous Piobbico core. Thanks also go to Dmitry Bazykin, who contributed hard-won data from the Malyi Karatau of Kazhakstan, to Ralf Tiedemann for providing ODP Site 659 data, and to Paul Olsen and Nick Shackleton for providing full documentation of their data on their public domain ftp sites.

LITERATURE CITED

Anderson RY. 1982. A long geoclimatic record from the Permian. *J. Geophys. Res.* 87(C9):7285–94

Anderson RY, Dean WE. 1995. Filling the Delaware Basin: hydrologic and climatic controls on the Upper Permian Castile Formation varved evaporite. In *The Permian of Northern Pangea, Vol. 2: Sedimentary Basins and Economic Resources*, ed. PA Scholle, TM Peryt, DS Ulmer-Scholle, pp. 61–78. Berlin: Springer-Verlag

Allen BD, Anderson RY. 1993. Evidence from western North America for rapid shifts in climate during the last glacial maximum. *Science* 260:1920–23

Allen JRL, Hoskins BJ, Sellwood BW, Spicer RA, Valdes PJ. 1993. Palaeoclimates and their modelling with special reference to the Mesozoic Era. *Phil. Trans. R. Soc. Lond., Series B* 341:203–343

Barrell J. 1917. Rhythms and measurement of geological time. *Geol. Soc. Am. Bull.* 28:275–304

Bartolini A, Baumgartner PO, Hunzer J. 1996. Middle and Late Jurassic carbon stable-isotope stratigraphy and radiolarite sedimentation of the Umbria-Marche basin

(Central Italy). *Ecol. Geol. Helv.* 89:811–44

Bazykin DA. 1997. *The origin of depositional cycles in shallow marine carbonates: an approach using coupled computer modelling and time series analysis.* Ph.D. dissertation, Johns Hopkins University, Baltimore, Maryland. 374 pp.

Bazykin DA, Demicco RV, Hardie LA. 1997. Autocycles vs. allocycles in shallow marine carbonate platform deposits: insights from 2-dimensional computer modelling experiments. *Gaea Heidelbergensis* 3:66

Bazykin DA, Hinnov LA. 2000. Orbitally-driven depositional cyclicity of the Lower Paleozoic Aisha-Bibi seamount (Malyi Karatau, Kazakstan): integrated sedimentological and time series study. *SEPM Special Publication: Carbonates of the CIS.* In press

Beaufort L. 1994. Climatic importance of the modulation of the 100 kyr cycle inferred from 16 m.y. long Miocene records. *Paleoceanography* 9:821–34

Behl RJ, Kennett JP. 1996. Brief interstadial events in the Santa Barbara basin, NE Pacific, during the last 60 kyr. *Nature* 379:243–46

Bellanca A, Claps M, Erba E, Masetti D, Neri R, et al. 1996. Orbitally induced limestone/marlstone rhythms in the Albian-Cenomanian Cismon section (Venetian region, northern Italy); sedimentology, calcareous and siliceous plankton distribution, elemental and isotope geochemistry. *Palaeogeogr. Palaeoclimatol. Palaeoecol.* 126(3–4):227–60

Berger A. 1977. Long-term variations of the Earth's orbital elements. *Celestial Mech.* 15:53–74

Berger A. 1978a. A simple algorithm to compute long term variations of daily or monthly insolation. *Contribution no. 18,* Institut d'Astronomie et de Géophysique G. Lemaître, Université Catholique de Louvain, Louvain-la-Neuve. 37 pp.

Berger A. 1978b. Long-term variations of daily insolation and Quaternary climatic changes. *J. Atmos. Sci.* 35(12):2362–67

Berger A. 1996. Comments to ''Insolation in terms of Earth's orbital parameters.'' *Theor. Appl. Climatol.* 53:253–55

Berger A, Li XS, Loutre M-F. 1999. Modelling Northern Hemisphere ice volume over the last 3 Ma. *Quat. Sci. Rev.* 18:1–11

Berger A, Loutre M-F. 1988. New insolation values for the climate of the last 10 million years. *Sci. Report 1988/13,* Institut d'Astronomie et de Géophysique G. Lemaître, Université Catholique de Louvain, Louvain-la-Neuve. 25 pp.

Berger A, Loutre M-F. 1990. Origine des fréquences des éléments astronomiques intervenant dans le calcul de l'insolation. *Bull. Cl. Sci. Acad. R. Belg.* 6(1):45–106

Berger A, Loutre M-F. 1991. Insolation values for the climate of the last 10 million years. *Quat. Sci. Rev.* 10:297–317

Berger A, Loutre M-F. 1994. Astronomical forcing through geologic time. In *Orbital Forcing and Cyclic Sequences,* ed. PL DeBoer, DG Smith, Spec. Publ. 19, Int. Ass. Sed., pp. 15–24. Oxford: Blackwell Scientific

Berger A, Loutre M-F. 1997. Intertropical latitudes and precessional and half-precessional cycles. *Science* 278:1476–78

Berger A, Loutre M-F, Dehant V. 1989. Influence of the changing lunar orbit on the astronomical frequencies of pre-Quaternary insolation patterns. *Paleoceanography* 4(5): 555–64

Berger A, Loutre M-F, Laskar J. 1992. Stability of the astronomical frequencies over the Earth's history for paleoclimatic studies. *Science* 255:560–66

Berger A, Loutre M-F, Mélice JL. 1998. Instability of the astronomical periods from 1.5 Myr BP to 0.5 Myr AP. *Paleoclimates* 2(4):239–80

Berger A, Loutre M-F, Tricot C. 1993. Insolation and Earth's orbital periods. *J. Geophys. Res.* 98(D6):10341–62

Berger A, Melice J-L, Hinnov L. 1991. A strategy for frequency spectra of Quaternary climate records. *Climate Dyn.* 5:227–40

Berggren WA, Kent DV, Swisher CC, Aubry M-P. 1995. A revised Cenozoic geochronology and chronostratigraphy. In *Geochronology, Time Scales and Global Stratigraphic Correlation*, ed. WA Berggren, DV Kent, M-P Aubry, J Hardenbol. SEPM Spec. Pub. 54:129–212

Bills BG. 1990. The rigid body obliquity history of Mars. *J. Geophys. Res.* 95(B9): 14137–53

Bolton EW, Maasch KA, Lilly JM. 1995. A wavelet analysis of Plio-Pleistocene climate indicators: a new view of periodicity evolution. *Geophys. Res. Lett.* 22:2753–56

Bond G, Broecker W, Lotti R, McManus JF. 1992. Abrupt color changes in isotope stage 5 in North Atlantic deep sea cores: implications for rapid change of climate-driven events. In *Start of a Glacial*, NATO ASI Series I, ed. G Kukla, E Went, 3:185–205

Bond G, Showers W, Cheseby M, Lotti R, Almasi P, et al. 1997. A pervasive millennial-scale cycle in North Atlantic Holocene and glacial climates. *Science* 278:1257–66

Bond GC, Kominz MA, Beaven J. 1991. Evidence for orbital forcing of Middle Cambrian peritidal cycles: Wah Wah range, south-central Utah. In *Sedimentary Modeling: Computer Simulations and Methods for Improved Parameter Definition*, ed. EK Franseen, WL Watney, DG StC Kendall, W Ross. Kansas Geological Survey Bulletin No. 233, pp. 293–317

Bowring SA, Grotzinger JP, Isachsen CE, Knoll AH, Pelechaty S, Kolosov P. 1993. Calibrating rates of early Cambrian evolution. *Science* 261:1293–98

Bracewell RN. 1965. *The Fourier Transform and Its Applications.* New York: McGraw-Hill. 381 pp.

Brack P, Mundil R, Meier M, Oberli F, Rieber H. 1996. Biostratigraphic and radiometric age data question the Milankovitch characteristics of the Latemar cycles. *Geology* 24:371–75

Brack P, Mundil R, Meier M, Oberli F, Rieber H. 1997. Biostratigraphic and radiometric age data question the Milankovitch characteristics of the Latemar cycles—Reply. *Geology* 25:471–72

Bradley RS. 1999. *Paleoclimatology: Reconstructing Climates of the Quaternary.* International Geophysics Series No. 64. London: Academic. 612 pp.

Bretagnon P. 1974. Termes à longues périodes dans le système solaire. *Astron. Astrophys.* 30:141–54

Bretagnon P. 1984. Accuracy of long term planetary theory. In *Milankovitch and Climate, Part 1*, ed. A Berger, J Imbrie, J Hays, G Kukla, B Saltzman, pp. 41–54. Dordrecht: Reidel

Broecker WS, Denton GH. 1989. The role of ocean-atmosphere reorganizations in glacial cycles. *Geochim. Cosmochim. Acta* 53:2465–501

Brüggemann W. 1992. A minimal cost function method for optimizing the age-depth relation of deep sea sediment cores. *Paleoceanography* 7(4)467–87

Cannariato KG, Kennett JP. 1999. Climatically related millennial-scale fluctuations in strength of California margin oxygen-minimum zone during the past 60 k.y. *Geology* 27(11):975–78

Cerveny RS. 1991. Orbital signals in the diurnal cycle of radiation. *J. Geophys. Res.* 96(D9):17209–15

Clement AC, Seager R, Cane MA. 1999. Orbital controls on the El Niño/Southern Oscillation and the tropical climate. *Paleoceanogr.* 14(4):441–56

Coccioni R, Galeotti S. 1991. Orbitally induced cycles in bentonic foraminiferal assemblage distribution from the Aptian-Apbian organic-rich Scisti a Fucoidi (Central Italy). *IGCP Meeting 262—Pelagic Facies*, Grenoble, pp. 1–2

Crowley T, North G. 1991. *Paleoclimatology.* Oxford, UK: Oxford Univ. Press. 339 pp.

Dansgaard W, Johnsen SJ, Clausen HB, Dahl-Jensen D, Gundestrup N, et al. 1993. Evidence for general instability of past climate from a 250-kyr ice-core record. *Nature* 364:218–20

D'Argenio B, Fischer AG, Richter GM, Longo G, Pelosi N, et al. 1998. Orbital cyclicity in the Eocene of Angola: visual and image-time-series analysis compared. *Earth Planet. Sci. Lett.* 160:147–61

De Boer PL. 1982. Cyclicity and the storage of organic matter in Middle Cretaceous pelagic sediments. In *Cyclic and Event Stratification,* ed. G Einsele, A Seilacher, pp. 456–75. Berlin: Springer-Verlag

DeMenocal PG, Bloemendal J, King JW. 1991. A rock magnetic record of monsoonal dust deposition to the Arabian Sea: evidence for a shift in the mode of deposition at 2.4 Ma. *Sci. Results ODP* 117:389–407

Demicco RV. 1998. CYCOPATH-2D—a two-dimensional, forward model of cyclic sedimentation on carbonate platforms. *Comput. Geosci.* 24(5):405–24

Dickey J, et al. 1994. 1994 Lunar laser ranging: a continuing legacy of the Apollo program. *Science* 265:182–90

Droxler AW, Schlager W. 1985. Glacial versus interglacial sedimentation rates and turbidite frequency in the Bahamas. *Geology* 13:799–802

Drummond CN, Wilkinson BH. 1993. On the use of cycle thickness diagrams as records of long-term sealevel change during accumulation of carbonate sequences. *J. Geol.* 101:687–702

Einsele G, Ricken W, Seilacher A. 1991. Cycles and events in stratigraphy—basic concepts and terms. In *Cycles and Events in Stratigraphy,* ed. G Einsele, W Ricken, A Seilacher, pp. 1–19. Berlin: Springer-Verlag

Elrick M, Hinnov LA. 1996. Millennial scale climate origins for stratification in Cambrian and Devonian deep-water rhythmites, western USA. *Palaeogeogr. Palaeoclimatol. Palaeoecol.* 123:353–72

Elrick M, Read JF, Coruh C. 1991. Short-term paleoclimatic fluctuations expressed in Lower Mississippian ramp-slope deposits, southwestern Montana. *Geology* 19:799–802

Erba E, Premoli Silva I. 1994. Orbitally driven cycles in trace-fossil distribution from the Piobbico core (Late Albian, central Italy). In *Orbital Forcing and Cyclic Sequences,* ed. PL DeBoer, DG Smith, pp. 211–26. Spec. Publ. 19, Int. Ass. Sed. Oxford: Blackwell Sci.

Fischer AG. 1964. The Lofer cyclothems of the Alpine Triassic. *Kansas Geol. Surv. Bull.* 169:107–49

Fischer AG. 1991. Orbital cyclicity in Mesozoic strata. In *Cycles and Events in Stratigraphy,* ed. G Einsele, W Ricken, A Seilacher, pp. 48–62. Berlin: Springer-Verlag

Fischer AG, Herbert TD, Napoleone G, Premoli-Silva I, Ripepe M. 1991. Albian pelagic rhythms (Piobbico Core). *J. Sediment. Petrol.* 61(7):1164–72

Gabor D. 1946. Theory of communication, part 1. *J. Inst. Elect. Eng.* 93(pt. 3):429–41

Ghil M, Taricco C. 1997. Advanced spectral analysis methods. In *Past and Present Variability of the Solar-Terrestrial System: Measurement, Data Analysis and Theoretical Models,* ed. G Cini Castagnoli, A Provenzale, pp. 137–59. Bologna: Società Italiana di Fisica

Goldhammer RK, Dunn PA, Hardie LA. 1987. High frequency glacio-eustatic oscillations with Milankovitch characteristics recorded in northern Italy. *Am. J. Sci.* 287:853–92

Goldhammer RK, Dunn PA, Hardie LA. 1990. Depositional cycles, composite sea-level changes, cyclic stacking patterns, and the hierarchy of stratigraphic forcing: examples from Alpine Triassic platform carbonates. *GSA Bull.* 102:535–62

Grippo A, Fischer AG, Hinnov LA, Pratt LM, Premoli Silva I. 1999. Cyclicity in bathyal Aptian-Albian sediments, Italy. *European Union of Geosciences,* Strasbourg, France. p. 237

Grippo A, Fischer AG, Hinnov LA, Premoli Silva I. 1998. Time-frequency analysis of cyclicity in a pelagic Aptian-Albian core from Piobbico, northern Apennines. *Geol.*

Soc. Am. Annual Meeting, Toronto. p. A-338

Grippo A, Hinnov L, Fischer A. 2000. Image processing and gray-scale scans in high resolution stratigraphy. *J. Sedim. Res.* In review

Grootes PM, Stuiver M, White JWC, Johnsen S, Jouzel J. 1993. Comparison of oxygen isotope records from the GISP2 and GRIP Greenland ice cores. *Nature* 366:552–54

Hagelberg T, Pisias N, Elgar S. 1991. Linear and nonlinear couplings between orbital forcing and the marine d18O record during the late Neogene. *Paleoceanography* 6(6):729–46

Hagelberg TK, Bond G, DeMenocal P. 1994. Milankovitch band forcing of sub-Milankovitch climate variability during the Pleistocene. *Paleoceanography* 9(4):545–58

Hanchar JM, Miller CF. 1993. Zircon zonation patterns as revealed by cathodoluminscence and backscattered electron images: implications for interpretation of complex crustal histories. *Chem. Geol.* 110:1–13

Hanchar JM, Rudnick RL. 1995. Revealing hidden structures; the application of cathodoluminescence and back-scattered electron imaging to dating zircons from lower crustal xenoliths. *Lithos* 36:289–303

Hardie LA, Hinnov LA. 1997. Biostratigraphic and radiometric age data question the Milankovitch characteristics of the Latemar cycles—Comment. *Geology* 25:470–71

Hays JD, Imbrie J, Shackleton NJ. 1976. Variations in the Earth's orbit: pacemaker of the ice ages. *Science* 194:1121–32

Hendy IL, Kennett JP. 1999. Latest Quaternary North Pacific surface-water responses imply atmosphere-driven climate instability. *Geology* 27(4):291–94

Herbert TD. 1992. Paleomagnetic calibration of Milankovitch cyclicity in Lower Cretaceous sediments. *Earth. Planet. Sci. Lett.* 112:15–28

Herbert TD. 1994. Reading orbital signals distorted by sedimentation: models and examples. In *Orbital Forcing and Cyclic Sequences*, ed. PL DeBoer, DG Smith, pp. 483–508. Spec. Publ. 19, Int. Ass. Sed. Oxford: Blackwell Sci.

Herbert TD, Burnett C, Tom BA. 1992. Precise major component determinations in deep-sea sediments using Fourier Transform infrared spectroscopy. *Geochim. Cosmochim. Acta* 59:1759–63

Herbert TD, Fischer AG. 1986. Milankovitch origin of mid-Cretaceous black shale rhythms in central Italy. *Nature* 321:739–43

Herbert TD, Mayer LA. 1991. Long climatic time series from sediment physical property measurements. *J. Sedim. Petrol.* 61(7): 1089–108

Herbert TD, Premoli Silva I, Erba E, Fischer A. 1995. Orbital chronology of Cretaceous-Paleocene marine sediments. In *Geochronology, Time Scales and Global Stratigraphic Correlation*, ed. WA Berggren, DV Kent, M-P Aubry, J Hardenbol. SEPM Spec. Pub. 54:81–94

Herbert TD, Stallard RF, Fischer AG. 1986. Anoxic events, productivity rhythms, and the orbital signature in a Mid-Cretaceous deep sea sequence from central Italy. *Paleoceanography* 1:495–506

Herterich K, Sarnthein M. 1984. Brunhes time scale: tuning by rates of calcium-carbonate dissolution and cross spectral analysis with solar insolation. In *Milankovitch and Climate, Part 1*, ed. A Berger, J Imbrie, J Hays, G Kukla, B Saltzman, pp. 447–66. NATO ASI Series. Dordrecht, The Netherlands: Reidel

Hilgen F, Abdul Aziz H, Krijgsman W, Langereis CG, Lourens LJ, et al. 1999. Present status of the astronomical (polarity) timescale for the Mediterranean Late Neogene. *Phil. Trans. R. Soc. Lond. A.* 357:1931–48

Hinnov LA, Cozzi A, Bazykin DA. 1997. The Milankovitch origin of the Middle Triassic Latemar platform cycles: a review of the sedimentolotgic criteria and results of a new evolutive spectral analysis of the entire Latemar cyclic succession. *Gaea Heidelbergensis* 3:164–65

Hinnov LA, Park JJ. 1998. Detection of astronomical cycles in the stratigraphic record by frequency modulation (FM) analysis. *J. Sedim. Res.* 68(4):524–39

Hinnov LA, Park JJ. 1999. Strategies for assessing Early-Middle (Pliensbachian-Aalenian) Jurassic cyclochronologies. *Phil. Trans. R. Soc. Lond. A.* 357:1831–60

Hinnov LA, Park JJ, Erba E. 2000. Lower-Middle Jurassic rhythmites from the Lombard Basin, Italy: a record of orbitally-forced cycles modulated by long-term secular environmental changes in west Tethys. In *Advances in Jurassic Research 2000*, ed. RL Hall, P Smith, pp. 437–54. Switzerland: Trans Tech

Hjelt S-E. 1992. *Pragmatic Inversion of Geophysical Data.* Lecture Notes in Earth Sciences. Berlin: Springer-Verlag. 262 pp.

Hooghiemstra H, Mélice J-L, Berger A, Shackleton NJ. 1993. Frequency spectra and paleoclimatic variability of the high-resolution 30–1450 ka Funza I pollen record (Eastern Cordillera, Colombia). *Quat. Sci. Rev.* 12(2):141–56

Imbrie J, Berger A, Boyle EA, Clemens SC, Duffy A, et al. 1993. On the structure and origin of major glaciation cycles: 2. The 100,000-year cycle. *Paleoceanography* 8(6):699–735

Imbrie J, Boyle EA, Clemens S, Duffy A, Howard W, et al. 1992. On the structure and origin of major glaciation cycles: 1. Linear responses to Milankovitch forcing. *Paleoceanography* 7:701–38

Jarrard RD, Arthur MA. 1989. Milankovitch paleoceanographic cycles in geophysical logs from ODP Leg 105, Labrador Sea and Baffin Bay. In *Proc. ODP, Sci. Results*, ed. SP Srivastava, M Arthur, B Clement, et al, 105:757–72

Jenkins GM, Watts DG. 1968. *Spectral Analysis and Its Applications.* San Francisco: Holden-Day. 525 pp.

Jenkyns HC. 1988. The early Toarcian (Jurassic) anoxic event: stratigraphic, sedimentary and geochemical evidence. *Am. J. Sci.* 288:101–51

Jouzel J, Lorius C, Petit JR, Genthon C, Barkov NI, et al. 1987. Vostok ice core: a continuous isotope temperature record over the last climatic cycle (160,000 years). *Nature* 329:403–8

Kaula WM. 1966. *Theory of Sattelite Geodesy.* Waltham, MA: Blaisdell. 124 pp.

Kerr RA. 1999. Geology near, far, and long ago. *Science* 286:1279–81

King T. 1996. Quantifying nonlinearity and geometry in time series of climate. *Quat. Sci. Rev.* 15(4):247–66

Koerschner WF, Read JF. 1989. Field and modelling studies of Cambrian carbonate cycles, Virginia Appalachians. *J. Sedim. Petrol.* 59(5):654–87

Kominz MA, Bond GC. 1990. A new method of testing periodicity in cyclic sediments: application to the Newark Supergroup. *Earth Planet. Sci. Lett.* 8:233–44

Kominz MA, Bond GC. 1992. Documenting the reliability and utility of the gamma method as applied to cyclic sections using forward modeling. *Earth Planet. Sci. Lett.* 113:449–57

Kominz MA, Heath GR, Ku TL, Pisias NG. 1979. Brunhes time scales and the interpretation of climatic change. *Earth Planet. Sci. Lett.* 45(2):394–410

Kukla G, An ZS, Melice J-L, Gavin J, Xiao JL. 1990. Magnetic susceptibility record of Chinese Loess. *Trans. R. Soc. Edinb.: Earth Sci.* 81:263–88

Kukla G, Cilek V. 1996. Plio-Pleistocene megacycles; record of climate and tectonics. *Palaeogeogr. Palaeoclimatol. Palaeoecol.* 120(1–2):171–94

Kunzel F. 1989. Maximum entropy spectral estimation: some new statistical and numerical details. *Beitr. Phys. Atmosph.* 62(3):227–35

Lambeck K. 1980. *The Earth's Variable Rotation: Geophysical Causes and Consequences.* Cambridge, UK: Cambridge University Press. 449 pp.

Larson RL, Erba E, Fischer AG, Premoli Silva I. 1993. *APTICORE-ALBICORE: A Workshop on Global Events and Rhythms of the Mid-Cretaceous.* Washington, DC: Joint Oceanographic Institutions. 56 pp.

Laskar J. 1988. Secular evolution of the solar system over 10 million years. *Astron. Astrophys.* 198:341–62

Laskar J. 1989. A numerical experiment on the chaotic behaviour of the solar system. *Nature* 338:237–38

Laskar J. 1990. The chaotic motion of the solar system: a numerical estimate of the size of the chaotic zones. *Icarus* 88:266–91

Laskar J. 1992. A few points on the stability of the Solar System. In *Chaos, Resonance and Collective Dynamical Phenomena in the Solar System*, ed. S Ferraz-Mello, pp. 1–16. Dordrecht, The Netherlands: Kluwer

Laskar J. 1999. The limits of Earth orbital calculations for geological time-scale use. *Phil. Trans. R. Soc. Lond. A.* 357:1735–59

Laskar J, Joutel F, Boudin F. 1993. Orbital, precessional and insolation quantities for the Earth from –20Myr to +10Myr. *Astron. Astrophys.* 270:522–33

Liu HS. 1992. Frequency variations of the Earth's obliquity and the 100-kyr ice-age cycles. *Nature* 358:396–99

Liu H-S. 1995. A new view on the driving mechanism of Milankovitch glaciation cycles. *Earth Planet. Sci. Lett.* 131:17–26

Liu H-S. 1998. Glacial-interglacial changes induced by pulse modulation of the incoming solar radiation. *J. Geophys. Res.* 103(D20):26147–64

Liu H-S. 2000. Insolation changes caused by combination of amplitude and frequency modulation of the obliquity. *J. Geophys. Res.* In press

Liu HS, Chao BF. 1998. Wavelet spectral analysis of the Earth's orbital variations and paleoclimatic cycles. *J. Atmos. Sci.* 55(2):227–36

Lourens LJ, Hilgen FJ. 1997. Long-period variations in the Earth's obliquity and their relation to third-order eustatic cycles and late Neogene glaciations. *Quat. Int.* 40:43–52

Lourens LJ, Hilgen FJ, Raffi I, Vergnaud-Grazzini C. 1996. Early Pleistocene chronology of the vrica section (Calabria, Italy). *Paleoceanogr.* 11:797–812

Lowell TV, Heusser CJ, Andersen BG, Moreno PI, Hauser A, et al. 1995. Interhemispheric correlation of Late Pleistocene glacial events. *Science* 269:1541–49

Mann ME, Lees JM. 1996. Robust estimation of background noise and signal detection in climatic time series. *Clim. Change* 35:409–45

Martinson DG, Menke W, Stoffa P. 1982. An inverse approach to signal correlation. *J. Geophys. Res.* 87:4807–48

Matthews RK, Frohlich C, Duffy A. 1997. Orbital forcing of global change throughout the Phanerozoic: a possible stratigraphic solution to the eccentricity phase problem. *Geology* 25(9):807–10

Melnyk DH, Smith DG, Amiri-Garroussi K. 1994. Filtering and frequency mapping as tools in subsurface cyclostratigraphy, with examples from the Wessex Basin, UK. In *Orbital Forcing and Cyclic Sequences*, ed. PL DeBoer, DG Smith, pp. 35–46. Spec. Publ. 19, Int. Ass. Sed. Oxford: Blackwell Sci.

Menke WH. 1989. *Geophysical Data Analysis: Discrete Inverse Theory, Rev. Ed.* International Geophysical Series, Vol. 45. New York: Academic. 289 pp.

Mezger K, Krogstad EJ. 1997. Interpretation of discordant U-Pb zircon ages; an evaluation. *J. Metamorph. Geol.* 15:127–40

Miller CF, Hatcher RD Jr, Harrison TM, Coath CD, Gorisch EB. 1998. Cryptic crustal events elucidated through zone imaging and ion microprobe studies of zircon, southern Appalachian Blue Ridge, North Carolina-Georgia. *Geology* 26:419–22

Mommersteeg HJPM, Loutre M-F, Young R, Hooghiemstra H. 1995. Orbital forced frequencies in the 975000 year pollen record

from Tenagi Philippon (Greece). *Clim. Dyn.* 11(1):4–24

Morrison LV, Stephenson FR. 1991. Changes in length of day; 500 BC to present. In Reversals, secular variation and dynamo theory: proceedings of the 2nd SEDI Symposium, ed. GA Glatzmaier, PH Roberts. *Geophys. Astrophys. Fluid Dyn.* 60:1–4

Muller RA, MacDonald GJ. 1995. Glacial cycles and orbital inclination. *Nature* 377:107–8

Muller RA, MacDonald GJ. 1997a. Spectrum of 100-kyr glacial cycle: orbital inclination, not eccentricity. *Proc. Natl. Acad. Sci. USA* 94:8329–34

Muller RA, MacDonald GJ. 1997b. Glacial cycles and astronomical forcing. *Science* 277:215–18

Mundil R, Brack P, Meier M, Rieber H, Oberli F. 1996. High resolution U-Pb dating of Middle Triassic volcaniclastics: time scale calibration and verification of tuning parameters for carbonate sedimentation. *Earth Planet. Sci. Lett.* 141:137–51

Murray N, Holman M. 1999. The origin of chaos in the outer solar system. *Science* 283:1877–81

Neeman BU. 1993. Orbital tuning of paleoclimatic records: a reassessment. *Report No. 39572, Lawrence Livermore Natl. Lab.* 37 pp.

Néron de Surgy O, Laskar J. 1997. On the long term evolution of the spin of the Earth. *Astron. Astrophys.* 318:975–89

North GR, Cahalan RF, Coakley JA. 1981. Energy balance climate models. *Rev. Geophys. Space Phys.* 19:91–121

Obradovich JD. 1993. A Cretaceous time scale. In *Evolution of the Western Interior Basin,* ed. WGE Caldwell, EG Kauffman, pp. 379–96. Geological Association of Canada, Spec. Paper 39

Olsen P. 1984. Periodicity of lake-level cycles in the Late Triassic Lockatong Formation of the Newark Basin (Newark Supergroup, New Jersey and Pennsylvania. In *Milankovitch and Climate, Part 1,* ed. A Berger, J Imbrie, J Hays, G Kukla, B Saltzman, pp. 129–46. Dordrecht, The Netherlands: Reidel

Olsen P. 1997. Stratigraphic record of the early Mesozoic breakup of Pangea in the Laurasia-Gondwana rift system. *Annu. Rev. Earth Planet. Sci.* 25:337–401

Olsen P, Kent DV. 1999. Long-period Milankovitch cycles from the Late Triassic and Early Jurassic of eastern North America and their implications for the calibration of the Early Mesozoic time-scale and the long-term behavior of the planets. *Phil. Trans. R. Soc. Lond. A.* 357:1761–86

Pagani M, Freeman KH, Arthur MA. 1999. Late Miocene atmospheric CO_2 concentrations and the expansion of C4 grasses. *Science* 285:876–79

Paillard D, Labeyrie L, Yiou P. 1996. Macintosh program performs time-series analysis. *EOS Transactions,* American Geophysical Union 77:379

Park J, Herbert TD. 1987. Hunting for paleoclimatic periodicities in a geologic time series with an uncertain time scale. *J. Geophys. Res.* 92:14027–40

Park J, Maasch KA. 1993. Plio-Pleistocene time evolution of the 100-kyr cycle in marine paleoclimate records. *J. Geophys. Res.* 198(B1):447–61

Pestiaux P, Duplessy JC, Berger A. 1987. Paleoclimatic variability at frequencies ranging from 1 cycle/10,000 years to 1 cycle/1,000 years: evidence for nonlinear behavior of the climate system. In *Climate—History, Periodicity and Predictability,* ed. MR Rampino, et al, pp. 285–99. New York: Van Nostrand Reinhold

Peterson I. 1993. *Newton's Clock: Chaos in the Solar System.* New York: Freeman. 317 pp.

Petit JR, Jouzel J, Raynaud D, Barkov NI, Barnola J-M, et al. 1999. Climate and atmospheric history of the past 420,000 years from the Vostok ice core, Antarctica. *Nature* 399:429–36

Pisias NG, Moore TC. 1981. The evolution of Pleistocene climate: a time series approach. *Earth Planet. Sci. Lett.* 52:450–58

Priestley MB. 1981. *Spectral Analysis and Time Series*, Vols. 1 and 2. London: Academic. 890 pp.

Prokoph A, Barthelmes F. 1996. Detection of nonstationarities in geological time series: Wavelet transform of chaotic and cyclic sequences. *Comput. Geosci.* 22(10):1097–108

Quinn TR, Tremaine S, Duncan M. 1991. A three million year integration of the Earth's orbit. *Astron. J.* 101:2287–305

Rial J. 1995. On the origin of the long period sawtooth shape of the late Pleistocene paleoclimate records: the first derivative of the earth's orbital eccentricity. *Geophys. Res. Lett.* 22(15):1997–2000

Rial J. 1999. Pacemaking the ice ages by frequency modulation of Earth's orbital eccentricity. *Science* 285:564–68

Ridgwell A, Watson A, Raymo ME. 1999. Is the spectral signature of the 100 kyr glacial cycle consistent with a Milankovitch origin? *Paleoceanography* 14(4):437–40

Ripepe M, Fischer AG. 1991. Stratigraphic rhythms synthesized from orbital variations. In *Sedimentary Modeling: Computer Simulations and Methods for Improved Parameter Definition,* ed. EK Franseen, WL Watney, DG StC Kendall, W Ross, pp. 335–44. Kansas Geological Survey Bulletin No. 233

Rowe HE. 1965. *Signal and Noise in Communication Systems.* New York: Van Nostrand Reinhold. 341 pp.

Rubincam DP. 1994. Insolation in terms of Earth's orbital parameters. *Theor. Appl. Climatol.* 48:195–202

Rubincam DP. 1996. Reply to comment on ''Insolation in terms of Earth's orbital Parameters.'' *Theor. Appl. Climatol.* 53:257–58

Sadler PM. 1981. Sediment accumulation rates and the completeness of stratigraphic sections. *J. Geol.* 89:569–684

Sadler PM. 1993. Time scale dependence of the rates of unsteady geologic processes. In *Rates of Geologic Processes, Tectonics, Sedimentation, Eustasy and Climate*, ed. JM Armentrout, R Bloch, HC Olson, BF Perkins. GCS SEPM, Res. Conf. 14:221–28

Sadler PM. 1994. The expected duration of upward-shallowing peritidal carbonate cycles and their terminal hiatuses. *Geol. Soc. Am. Bull.* 106:791–802

Sadler PM. 1999. The influence of hiatuses on sediment accumulation rates. In *On the Determination of Sediment Accumulation Rates*, ed. P Bruns, HC Hass, pp. 15–40. GeoResearch Forum, Vol. 5. Switzerland: Trans Tech

Saltzman B, Maasch K. 1990. A first order global model of Cenozoic climatic change. *Trans. R. Soc. Edinburgh: Earth Sci.* 81:315–25

Saltzman B, Sutera A. 1987. The mid-Quaternary climate transition as the free response of a three-variable system. *J. Atmos. Sci.* 44:236–41

Saltzman B, Verbitsky MYa. 1993. Multiple instabilities and modes of glacial rhythmicity in the Plio-Pleistocene: a general theory of late Cenozoic climatic change. *Clim. Dyn.* 9:1–15

Schwarzacher W. 1947. Über die Sedimentäre Rhythmik des Dachsteinkalkes von Lofer. *Verh. Geol. Bundesanst.* 1947:175–88

Schwarzacher W. 1993. *Cyclostratigraphy and the Milankovitch Theory.* Developments in Sedimentology 52. Amsterdam: Elsevier. 225 pp.

Schwarzacher W, Fischer AG. 1982. Limestone-shale bedding and perturbations in the earth's orbit. In *Cyclic and Event Stratification,* ed. G Einsele, A Seilacher, pp. 72–95. Berlin: Springer-Verlag

Shackleton NJ, Crowhurst SJ, Weedon GP, Laskar J. 1999b. Astronomical calibration of Oligocene-Miocene time. *Phil. Trans. R. Soc. Lond. A.* 357:1907–30

Shackleton NJ, King Hagelberg T, Crowhurst SJ. 1995. Evaluating the success of astronomical tuning: pitfalls of using coherence as a criterion for assessing pre-Pleistocene timescales. *Paleoceanography* 10(4):693–97

Shackleton NJ, McCave IN, Weedon GP. 1999a. Preface. *Phil. Trans. R. Soc. Lond. A.* 357:1733–34

Short DA, Mengel JG, Crowley TJ, Hyde WT, North GR. 1991. Filtering of Milankovitch cycles by Earth's geography. *Quat. Res.* 35:157–73

Sussmann GJ, Wisdom J. 1992. Chaotic evolution of the solar system. *Science* 257:56–62

Taner MT, Koehler F, Sheriff RE. 1979. Complex trace analysis. *Geophysics* 44(6):1041–63

Thompson LG, Yao T, Davis ME, Henderson KA, Mosley-Thomson E, et al. 1997. Tropical climate instability: the last glacial cycle from a Qinghai-Tibetan ice core. *Science* 276:1821–25

Thomson DJ. 1982. Spectrum estimation and harmonic analysis. *Proc. IEEE* 70:1055–96

Thomson DJ. 1990. Time series analysis of Holocene climate data. *Phil. Trans. R. Soc. Lond. A.* 330:601–16

Thomson DJ. 1991. Quadratic-inverse spectrum estimates: applications to palaeoclimatology. *Phil. Trans. R. Soc. Lond. A.* 322:539–97

Touma J, Wisdom J. 1994. Evolution of the Earth-Moon system. *Astron. J.* 108:1943–61

Torrence C, Compo GC. 1998. A practical guide to wavelet analysis. *Bull. Am. Meteor. Soc.* 79:61–78

Tricot C, Berger A. 1988. Sensitivity of present-day climate to astronomical forcing. In *Long and Short-Term Variability of Climate*, Vol. 16, *Lectures in Earth Sciences*, ed. H Wanner, U Siegenthaler, pp. 132–52. New York: Springer-Verlag

Tiedemann R, Sarnthein M, Shackleton NJ. 1994. Astronomical timescale for the Pliocene Atlantic δ18O and dust flux records of ODP Site 659. *Paleoceanography* 9:619–38

Weedon GP. 1989. The detection and illustration of regular sedimentary cycles using Walsh power spectra and filtering, with examples from the Lias of Switzerland. *J. Geol. Soc.* 146:133–44

Weedon GP, Shackleton NJ, Pearson PN. 1997. The Oligocene time scale and cyclostratigraphy on the Ceara Rise, Western Equatorial Atlantic. In *Proc. ODP, Sci. Results*, ed. NJ Shackleton, WB Curry, C Richter, TJ Bralower. 154:101–14

Wilkinson BH, Diedrich NW, Drummond CN, Rothman ED. 1998. Michigan hockey, meteoric precipitation, and rhythmicity of accumulation on peritidal carbonate platforms. *Geol. Soc. Am. Bull.* 110(8):1075–93

Williams DF, Peck J, Karabanov EG, Prokopenko AA, Kravchinsky V, et al. 1997. Lake Baikal record of continental climate response to orbital forcing during the past 5 million years. *Science* 278:1114–17

Willis KJ, Kleczkowski A, Briggs KM, Gilligan CA. 1999. The role of sub-Milankovitch climatic forcing in the initiation of the Northern Hemisphere glaciation. *Science* 285:568–71

Winograd IJ, Coplen TB, Landwehr JM, Riggs AC, Ludwig KR, et al. 1992. Continuous 500,000-year climate record from vein calcite in Devil's Hole, Nevada. *Science* 258:255–60

Woronow A. 1992. A test of the γ method for evaluating the periodicity of cyclical sediments. *Earth Planet. Sci. Lett.* 113:443–47

Yang W, Harmsen F, Kominz MA. 1995. Quantitative analysis of cyclic peritidal carbonate sequence, the Middle and Upper Devonian Lost Burro Formation, Death Valley, California: a possible record of Milankovitch climatic cycles. *J. Sedim. Res.* 65(3):306–22

Zempolich WG, Erba E. 2000. Sedimentologic and chemostratigraphic recognition of third-order sequences in resedimented carbonate: the Middle Jurassic Vajont Limestone, Venetian Alps, Italy. In *Advances in Carbonate Sequence Stratigraphy: Application to Reservoirs, Outcrops and Models*, SEPM Spec. Pub. No. 62. Tulsa, OK: Society of Sedimentary Geology. 36 pp. In press

Annual Review of Earth and Planetary Science
Volume 28, 2000

CONTENTS